BRNO UNIVERSITY OF TECHNOLOGY
VYSOKÉ UČENÍ TECHNICKÉ V BRNĚ

FACULTY OF MECHANICAL ENGINEERING
FAKULTA STROJNÍHO INŽENÝRSTVÍ

ENERGY INSTITUTE
ENERGETICKÝ ÚSTAV

VIZUALIZATION AND OPTICAL MEASUREMENTS OF TWO-PHASE FLOWS FOR PRESSURE-SWIRL ATOMIZER

VIZUALIZACE A OPTICKÁ MĚŘENÍ VNITŘNÍHO A VNĚJŠÍHO DVOUFÁZOVÉHO PROUDĚNÍ U TLAKOVÝCH VÍŘIVÝCH TRYSEK

MASTER'S THESIS
DIPLOMOVÁ PRÁCE

AUTHOR — **Bc. Lada Janáčková**
AUTOR PRÁCE

SUPERVISOR — **doc. Ing. Jan Jedelský, Ph.D.**
VEDOUCÍ PRÁCE

BRNO 2018

VYSOKÉ UČENÍ TECHNICKÉ V BRNĚ
FAKULTA STROJNÍHO INŽENÝRSTVÍ

Zadání diplomové práce

Ústav:	Energetický ústav
Studentka:	**Bc. Lada Janáčková**
Studijní program:	Strojní inženýrství
Studijní obor:	Technika prostředí
Vedoucí práce:	**doc. Ing. Jan Jedelský, Ph.D.**
Akademický rok:	2017/18

Ředitel ústavu Vám v souladu se zákonem č. 111/1998 o vysokých školách a se Studijním a zkušebním řádem VUT v Brně určuje následující téma diplomové práce:

Vizualizace a optická měření vnitřního a vnějšího dvoufázového proudění u tlakových vířivých trysek

Stručná charakteristika problematiky úkolu:

Tvorba spreje u tlakové vířivé trysky je komplexní proces dvoufázového proudění. Výsledný sprej podstatně závisí na charakteru vnitřního proudění v trysce. Bude provedena vizualizace a měření pomocí optických metod, se zaměřením na vnitřní vířivé proudění, výtok a primární rozpad kapalného filmu. Bude použit průhledný model trysky (studium charakteru vnitřního toku a chování vzdušného jádra, měření rychlostního profilu apod.) a reálná tlaková tryska (primární rozpad filmu). Součástí práce bude příprava experimentu (nastavení měřicích systémů, volba vnášených částic), vyhodnocení dat a grafická prezentace výsledků. Doporučené přístroje jsou: vysokorychlostní (VR) kamera, PIV a LDA.

Cíle diplomové práce:

1. Rozbor požadavků na uspořádání experimentu s vnitřním prouděním kapaliny pro aplikaci optických měření, požadavky na trasovací částice
2. Provedení vizualizace vnitřního a vnějšího proudění VR kamerou a měření rychlosti vnitřního proudění metodou LDA pro několik režimů trysky
3. Vyhodnocení rychlostního pole uvnitř trysky (střední a fluktuační složky rychlosti), analýza rychlostních profilů s ohledem na proudové struktury (LDA)
4. Kvalitativní popis tvaru vzdušného jádra a charakteru časových fluktuací vzdušného jádra, vyhodnocení jeho geometrie - průměr v několika polohách (VR kamera)
5. Tracking trasovacích částic, vyhodnocení jejich trajektorie (proudnice) a rychlosti pohybu, analýza rychlostního pole a porovnání s daty z LDA měření
6. Výtok z trysky - vyhodnocení úhlu kužele kapalného filmu
7. Analýza primárního rozpadu kapalného filmu na výstupu z trysky, popis průběhu rozpadu kapalného

filmu, jeho klasifikace a vyhodnocení vzdálenosti primárního rozpadu (VR kamera)

Seznam doporučené literatury:

SMITS, A. J. a LIM, T. T. Flow Visualization: Techniques and examples. London: Imperial College Press, 2003. ISBN 1-86094-193-1.

LEFEBVRE, Arthur H. a Vincent G. MCDONELL. Atomization and sprays. Second edition. Boca Raton: Taylor & Francis, CRC Press, 2017.

ĎURDINA, L. Metody vizualizace proudění. Brno: Vysoké učení technické v Brně, Fakulta strojního inţenýrství, 2010. 45 s.

NAKAYAMA, Y. a R. F. BOUCHER. Introduction to fluid mechanics. New York: J. Wiley, c1999.

LIN, S.-P. Breakup of liquid sheets and jets. New York: Cambridge University Press, 2003. ISBN 0521806941.

Termín odevzdání diplomové práce je stanoven časovým plánem akademického roku 2017/18.

V Brně, dne 25. 10. 2017

VYSOKÉ UČENÍ TECHNICKÉ V BRNĚ FAKULTA STROJNÍHO INŽENÝRSTVÍ DĚKANÁT

L. S.

doc. Ing. Jiří Pospíšil, Ph.D.
ředitel ústavu

doc. Ing. Jaroslav Katolický, Ph.D.
děkan fakulty

Abstract

The present thesis deals with a study of both Simplex and SR versions of the original atomizer used in a combustion chamber of the small turbojet engine. For a better understanding of the spray formation process, a transparent model of both atomizers was manufactured in the scale of 10:1. The spray formation of a pressure swirl atomizer is a complex process of the two-phase flow. The internal and external flow was examined using Laser Doppler Anemometry and a high-speed imaging at inlet pressures of Δp = 0.5, 1.0 and 1.5 MPa with the use of kerosene and p-Cymene as working liquids. In terms of internal flow, the air core characteristic was performed, and the influence of different SFR values on the air core length and diameter was investigated. The velocity profiles of the internal flow together with their fluctuation components have been further clarified, considering Reynolds number and used liquid. Also, the simple numerical model was developed to estimate the internal flow field by particle tracking. In the case of external flow, the dependence of the inlet pressure on the liquid sheet breakup length and the spray cone angle was investigated.

Keywords

Two-phase flow, internal flow, pressure-swirl, spill-return, scaled atomizer, air core.

Abstrakt

Tato práce se zabývá studií Simplex a SR verze původní trysky používané ve spalovací komoře malého proudového motoru. Pro lepší porozumění procesu rozprašování byl vyroben transparetní model obou trysek v měřítku 10:1. Tvorba spreje u tlakové vířivé trysky je komplexní proces dvoufázového proudění. Vnitřní a vnější proudění bylo zkoumáno pomocí Laserového Dopplerovského Anemometru a vysokorychlostní kamery při vstupních tlacích Δp = 0.5, 1.0 a 1.5 MPa s použitím kerosinu a p-Cymenu. Z hlediska vnitřního proudění byla provedena charakteristika vzdušného jádra a zkoumán vliv různých SFR hodnot na délku a průměr jádra. Dále byly objasněny rychlostní profily společně s jejich fluktuačními složkami vzhledem k Reynoldsovu číslu a použité kapalině. Také jednoduchý numerický model byl vyvinut k odhadu vnitřního proudění pomocí trackování částic. V případě vnějšího proudění byl zkoumán vliv vstupního tlaku na rozpadovou vzdálenost spreje a úhel kužele spreje.

Klíčová slova

Dvoufázové proudění, vnitřní proudění, tlaková vířivá, obtok, zvětšený model trysky, vzdušné jádro.

Bibliographic citation

JANÁČKOVÁ, L. *Vizualizace a optická měření vnitřního a vnějšího dvoufázového proudění u tlakových vířivých trysek.* Brno: Vysoké učení technické v Brně, Fakulta strojního inženýrství, 2018. 70 s. Vedoucí diplomové práce doc. Ing. Jan Jedelský, Ph.D.

Affirmation

I declare that this master's thesis is the result of my own work led by doc. Ing. Jan Jedelský, Ph.D. and all used sources are duly listed in the bibliography.

Bc. Lada Janáčková

Acknowledgments

Foremost, I would like to express my sincere gratitude to my supervisor doc. Ing. Jan Jedelský, Ph.D. for his guidance, motivation, and patience in difficult times. He was always willing to help me with problems I was facing.

I am also thankful that I had the opportunity to create this work with the support of the projects no. GA15-09040S and GA18-15839S funded by the Czech Science Foundation and LO1202 NETME CENTRE PLUS funded by the Ministry of Education, Youth and Sports of the Czech Republic under the National Sustainability Programme I.

I would like to express my thanks to Ing. Milan Malý for the help with preparation of measurement and for his valuable advice and comments.

Last, but not least, I would like to thank my parents, for the support they have provided me during my whole study.

Preface

Atomization is a process of breaking up a liquid into small droplets due to the interaction between the liquid and the ambient air. The resulting droplets form a spray generated by a device called an “atomizer” whose design depends on the application and operating conditions. In the past, many types of atomizers have been developed, but for the purpose of this thesis, pressure swirl atomizers have been used, which find application in combustion chambers of jet engines.

This work follows the author’s previous bachelor’s thesis [1], which deals with the visualization of flow at the atomizer exit. Quality of the resulting spray, however, significantly affects the character of the internal flow inside the atomizer. Therefore, this time the attention will be focused on both these processes.

Together with the visualization, which makes visible to the eye the invisible phenomena (e.g. the formation of the air core inside the atomizer, its stability, spray symmetry, etc.), optical methods (for measuring the velocity field of the atomizer or fluctuations) were also used. Appropriate selection and combination of these methods can achieve a more detailed understanding of the liquid breakup. Based on this information, it is possible to improve fuel atomization and thus increase the combustion efficiency.

Contents

1 Atomizers

Atomizers are devices used to spray the liquid into very small droplets. They find implementation in several industrial processes, e.g. mechanical, chemical, aerospace, pharmaceuticals, medicine, food processing, agriculture, environmental protection, meteorology, transportation, and others [2]. These examples are not complete, however, the importance of spray technology is obvious. This thesis is highly focused on small pressure-swirl atomizers intended for a turbojet engine. However, there are many other types of atomizers vary with design and energy used for atomization. An interested reader is referred to [3] or [4].

1.1 Pressure-swirl atomizers

Pressure-swirl (PS) atomizers are most commonly used in the field of combustion systems, water cooling etc. According to Malý [5], "the basic PS atomizer type is called 'simplex' due to the simplicity of its design". The principle relies on a conversion of the pressure energy into kinetic energy (velocity). In general, they consist of inlet tangential ports, a swirl chamber, and an exit orifice. A liquid is injected through tangential ports into a swirl chamber, thus acquires a swirling motion and creates the air core that extends from the exit orifice to the rear of the swirl chamber [4]. The liquid spreads out in the form of a hollow conical spray as soon as it leaves the exit orifice. According to Bayvel and Orzechowski [3], the main advantages are relatively simple construction, high reliability, good spraying quality and small power required. The major disadvantage is that doubling the flow rate demands a fourfold increase in injection pressure. This problem has been solved by developing the PS atomizers with a spill-line (the so-called spill-return atomizers), the duplex or the dual-orifice atomizers [5].

1.1.1 Spill-return atomizers

The spill-return (SR) atomizer is basically a simplex swirl atomizer that atomizes only a part of the working liquid. The liquid supplied to the swirl chamber is divided into two jets – one is discharged outside and atomized, the other is "spilled" back to the fuel tank through the annular slot in the rear wall of the swirl chamber. The advantages are simple to design and very good atomization quality in the wide range of flow rates [6]. On the other hand, the large variation in spray angle with a change in flow rate is the main disadvantage of this atomizer. [4,5,6]

1.2 Atomizer parameters

There are two important performance parameters which determine the suitability of the atomizer for a specific purpose – discharge coefficient and spray cone angle. [7]

1.2.1 Discharge coefficient

The discharge coefficient is defined as the ratio of actual to theoretical flow rate and it relates to the exit orifice. One of the first introduction of discharge coefficient was by Taylor [8] as:

$$C_D = \frac{Q}{A_O \left(\frac{\Delta p}{\rho_l}\right)^{0.5}} \tag{1}$$

where Q is flow rate, Ao is the cross-sectional area of the discharge orifice, Δp is the difference between the injection and back pressure, and ρ_l is the liquid density.

1.2.2 Spray cone angle

The spray cone angle (SCA) is an important aspect of the atomizer. It can affect the combustion efficiency, flame length and pollutant emission because an increase in the SCA leads to a greater exposure of the droplets to the surrounding air, which may result in improved atomization. [5,9] The characteristics of the flow in PSA have been studied by several workers [4,10,11]. Their results show that SCA is influenced mainly by the atomizer design, liquid properties, and the operating conditions. Scaling the nozzle permits scaling the flowrate, at constant spray angle.

2 Internal flow in atomizers

The swirling motion of the liquid inside the swirl chamber ensures that the liquid is forced away from the central axis and toward the side walls. The swirling liquid creates a low-pressure area in the center of the swirl chamber and generates an air core along the centerline. Within the atomizer, the air and liquid interface forms where the liquid pressure is approximately the same as the air outside the atomizer. According to Chinn and Yule [12], the air within the air core is carried out with the liquid and new air is sucked in, so the air core size and shape are constant approximately.

2.1 The air core characteristics

The internal flow characteristics were investigated by a few authors. Experimental studies of Som and Mukherjee [13], Datta and Som [14], and Khavkin [15] have established that the air core is relatively uniform throughout the converging part of the atomizer and it has a cylindrical shape with a little enlargement in the exit orifice, see Figure 2-1. This may be caused due to the change over from the confined to the unconfined nature of the flow with tangential velocity.

Halder et al. [16] investigated the shape of the air core in several transparent atomizers at various inlet mass flow rates of water. They found out that the formation of the air core depends on the inlet flow Reynolds number (*Re*). Two limiting values of *Re* were conducted. Only above the upper limit the air core was developed and stable; below the lower limit a full liquid stream exited the atomizer producing a solid cone spray instead of a hollow cone one and the air core was not formed. The air core was almost constant in diameter for large *Re* values, whereas for *Re* close to the limiting value its diameter increased with increasing *Re*. Lee et al. [17] also investigated the concept of limiting values of *Re*. They tested a transparent acrylic atomizer with both diesel and kerosene fuel under a range of inlet pressures and temperatures. The air core was stable for $Re_o > 3300$, for lower values the air core was unstable, and no air core was present for $Re_o < 2400$, due to insufficient centrifugal forces and the spray pulsed significantly. The *Re* values were related to the exit orifice. Löffler and Mang [18] investigated the behavior of the air core under the influence of various *spill-to-feed ratio* (SFR) in the case of SR atomizer. At an SFR = 0 the air core diameter increases towards the exit orifice, which corresponds to publications [19,12,13], whilst for SFR = 0.86 the air core assumes an almost cylindrical shape of very large diameter.

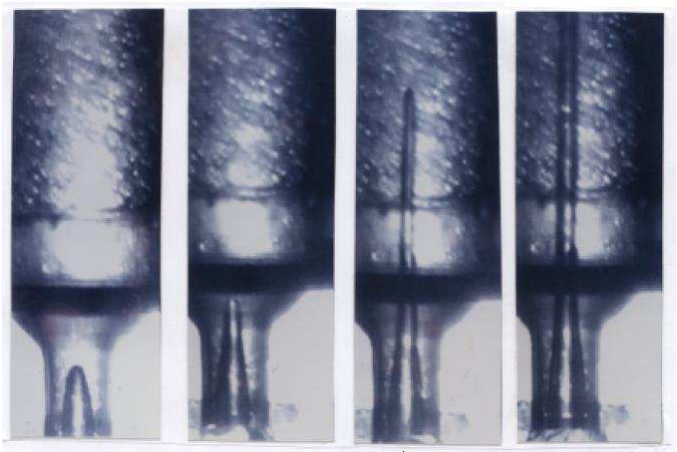

Figure 2-1 The developement of the air core inside the atomizer of Chinn. [11]

The air core size of the atomizer plays an important role in controlling the sheet thickness and primary breakup. The study by Som [20] shows, that the larger the diameter of the air core, the thinner the liquid film (sheet thickness), and, therefore, the smaller the droplet sizes. Ashgriz [21] further describes, that the air core reduces the effective flow area at the exit orifice and causes a reduction in the volumetric flow rate. Therefore, the larger the air core diameter, the smaller the discharge coefficient C_D.

2.2 Velocity profiles

In order to obtain better knowledge of the flow pattern inside the atomizer, the measurements of time mean velocities and turbulent fluctuations were earned out by LDA in the study of Horvay and Leuckel [22,23], who used the scaled transparent atomizer consisting of three parts: swirl generator, intermediate plate, and swirl chamber with exit orifice. To achieve the correct adaptation of the liquid and the Plexiglas material refraction index they used mixtures of tetrahydronaphthalene, ricinus, and turpentine oil, until the laser beam crosses fluid and Plexiglass material without being refracted. Due to the large difference in density between the seeding particles (small air bubbles) and fluid, no correct measurement of the radial velocity component was possible, hence only the axial and tangential velocity components were investigated. In the swirl chamber, a steady-state flow pattern is established with the inner free surface against the air core. The pattern of the tangential velocity is similar to a Rankine combined vortex. There is a smooth transition between two flow regimes of free-vortex and solid-body rotation, which make up the Rankine combined vortex. There are two peaks in the axial velocity profile, one near the air core and the other near the wall, see Figure 2-2. The tangential velocity profile behaves similarly, although it reached a sharper maximum near the air core. The velocity fluctuations reached their maximum values at those positions, where the gradients of the time mean velocities were high. These data were subsequently used by Chinn and Yule [12] and Cooper et al. [24] to compare with a numerical model. In both studies, the experimental data were in accordance with numeric. Moreover, Cooper [24] added the results of the radial component which was computed using mass continuity. In comparison with axial and tangential profiles, the radial component had the smallest values, see Figure 2-3. The resulting flow pattern of Krämer [25] and lately Löffler and Mang [18] was consistent with studies of previous authors, both in terms of velocity profiles and fluctuations, however, measurements with a higher viscosity test fluid resulted in lower fluctuations. Also, an influence of the SFR has been observed from the axial component profiles. At low SFR's two flow zones appeared (one at the atomizer periphery, the other near the air core), which merged with each

other in the region of the exit orifice. For very high SFR (SFR > 0.75) a back-flow along the air core was evident.

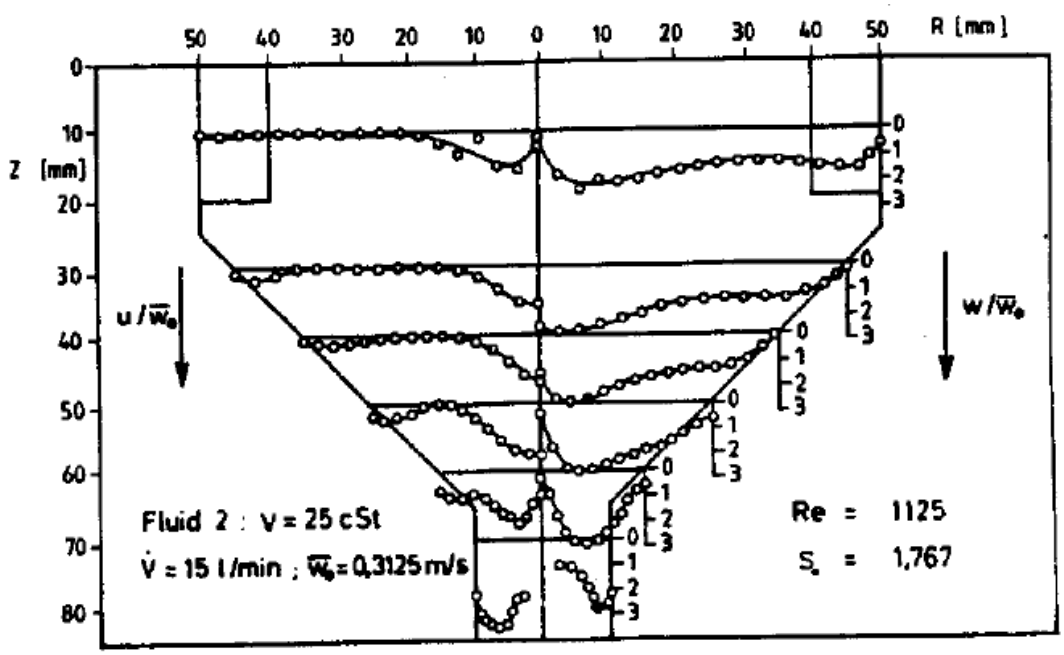

Figure 2-2 Axial (left) and tangential (right) velocity profiles for the concical atomizer of Horvay and Leuckel [23]

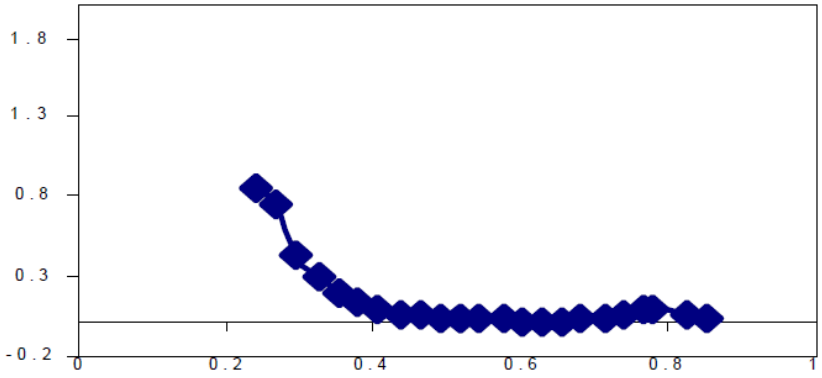

a) axial velocity profile

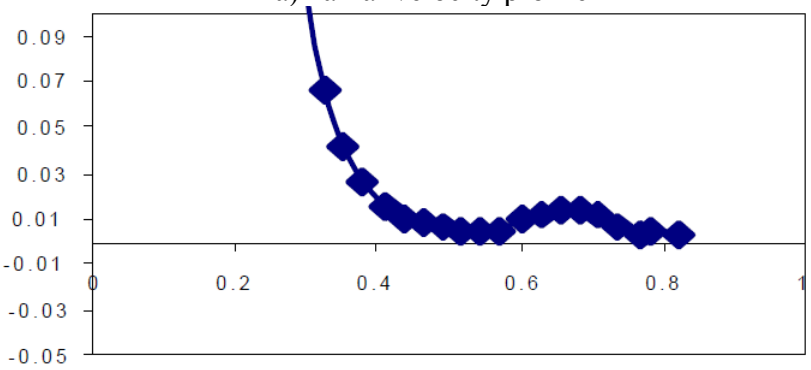

b) radial velocity profile

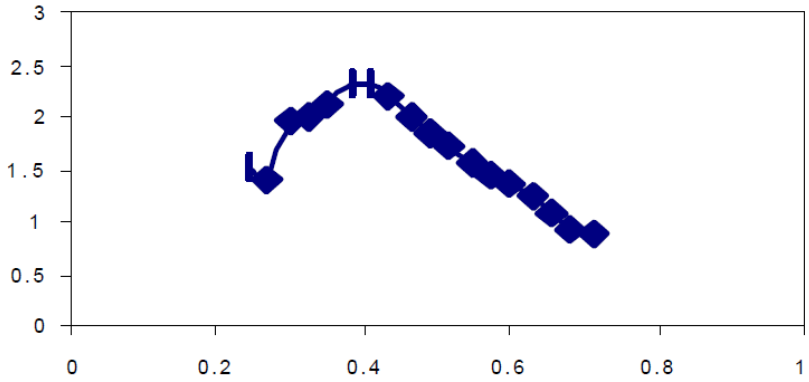

c) tangential velocity profile

Figure 2-3 Velocity profiles of Cooper et al. [24] at 17 mm from the swirl chamber exit

2.3 The liquid flow pattern

The fluid flow inside the swirl chamber has not been yet fully investigated. It is known that there is a swirling movement of fluid due to the tangential inlet ports. Also, velocity field of the fluid has already been received many times. Therefore, it can be assumed that even individual particles subjected to the liquid will be equally swirling if they have a low Stokes number. From the available literature, only Hansen [26] dealt with this in his thesis. He presented the liquid flow pattern of one particle inside the swirl chamber obtained from a numerical simulation, see Figure 2-4. The liquid enters the swirl chamber at the upper left-hand corner and is discharged through the exit orifice at the bottom. The gray part in the middle of the atomizer represents the air core. However, this was introduced without any further comments or explanations, apparently for demonstration only.

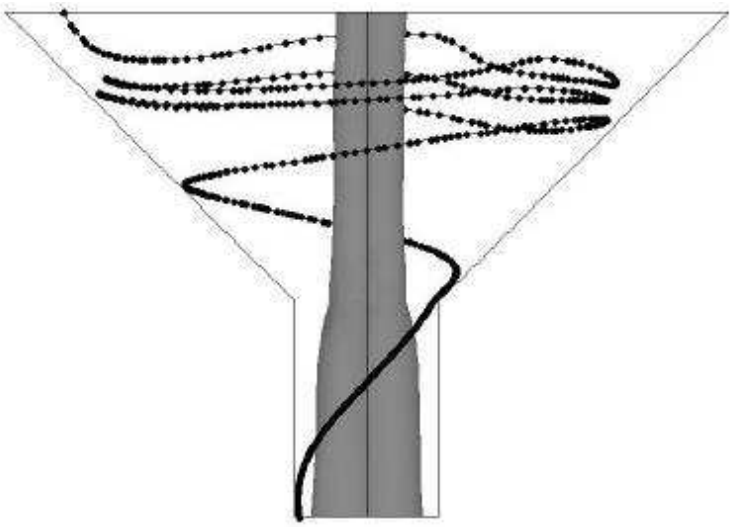

Figure 2-4 The liquid flow pattern inside the atomizer of Hansen [26]

3 External flow

Atomization is a process of breaking up a liquid into small droplets by the forces acting in or on the liquid surface. A good understanding of the liquid breakup mechanism is essential for raising the combustion efficiency and reducing the environmental pollution.

The process of atomization is much easier if the liquid is present in a form that is more susceptible to disintegration. This corresponds to thin liquid streams or sheets because they have the highest surface energy and thus the greatest instability. [3] The mechanisms of their breakup are clarified below.

3.1 Liquid stream breakup

A liquid stream issuing from the atomizer has a circular cross-section. As it is seen in Figure 3-1, near the atomizer the stream appears smooth and unperturbed, but after some distance downstream a small wavy disturbances appear. The difference between the velocity of the stream and the ambient air generates aerodynamic forces that amplify the waves on the stream surface. The waves grow in time and space until reaching critical amplitude and cause the liquid stream disintegration into large drops with a small single drop, referred to as "satellite" drop, between them. This theoretical assumption of liquid stream disintegration was first made by Rayleigh [27]. In his contribution, the liquid breakup occurs when the wavelength of the disturbances becomes equal to the perimeter of the stream.

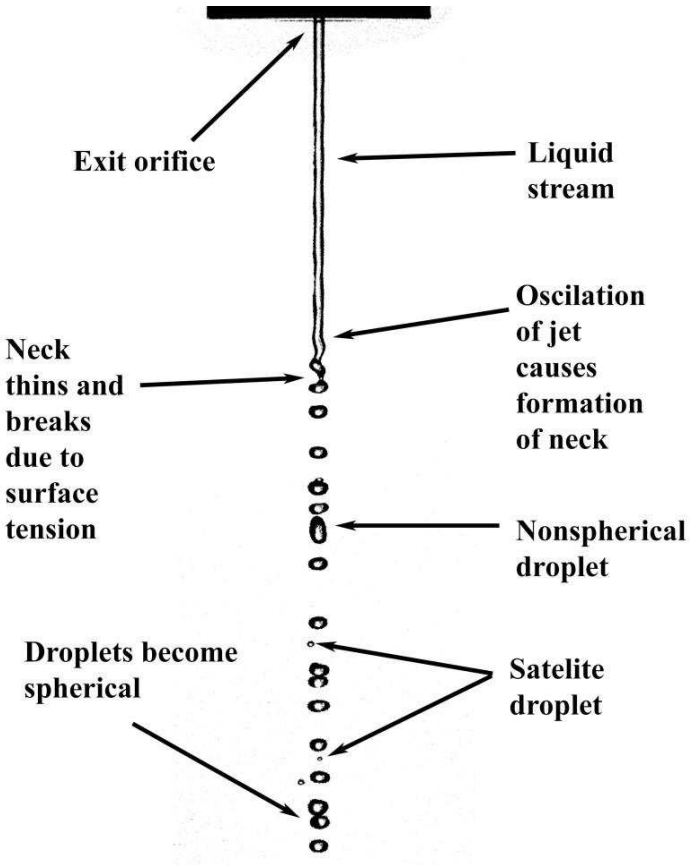

Figure 3-1 Liquid stream breakup

There are three important dimensionless numbers in the atomization process: Reynolds number, Weber number (*We*), and Ohnesorge number (*Oh*):

$$Re = \frac{\rho_l \cdot D \cdot v}{\mu_l} \tag{2}$$

$$We = \frac{\rho_l \cdot D \cdot V^2}{\sigma_l} \tag{3}$$

$$Oh = \frac{\sqrt{We}}{Re} = \frac{\mu_l}{\sqrt{\sigma_l \cdot \rho_l \cdot D}} \tag{4}$$

where D and v are the characteristic geometric parameter and velocity. These criteria are a function of the liquid density ρ_l, surface tension σ_l, and dynamic viscosity μ_l, which have already been described in [1].

The Reynolds number refers to the internal atomizer flow, and it describes the relationship between the inertial and the viscous forces. The Weber number represents the ratio of the inertia to surface tension forces. Combining these two numbers to eliminate the velocity, results in Ohnesorge number which represents fluid properties. It must be added that *We* and *Oh* refer to the external flow.

At low *Oh* and *Re* the aerodynamic interaction with surrounding air is neglectable, which corresponds to Rayleigh mechanism. Weber [28] extended Rayleigh‘s theory to the effect of viscosity on the liquid breakup. For Ohnesorge numbers $Oh < 0{,}1$, the effect of viscosity is negligible. [2] According to Bayvel and Orzechowski [3], the liquid breakup depends on the liquid velocity in the ambient air. With increasing liquid velocity, the liquid breakup starts immediately at the exit orifice and the droplets become smaller. It is related to Weber number. However, the influence of the exit orifice geometry, physical properties of the fluid and ambient medium cannot be ignored too.

3.2 Liquid sheet breakup

In many technical applications, the production of the conical liquid sheet is required rather than liquid stream. For example, in combustion engines, the fuel has to be injected in the form of very small droplets to ensure better and faster fuel combustion. Here, conical sheets are mostly generated by pressure swirl atomizers, where the liquid issues through one or more tangential passages thus getting swirling motion. According to Lefebvre [4], the atomization of spray consist of two main processes. Firstly, the liquid breaks up into various conical ligaments and large drops due to disruptive aerodynamic forces. This happens near the exit orifice and it is called *primary atomization*. However, the already mentioned structures are unstable and disintegrate again into very fine droplets in the process called *secondary atomization*, see Figure 3-2.

Many authors have investigated liquid sheet instabilities and factors influencing its breakup. According to Lin [29], the liquid sheet formation depends on *Re* and *We*, that depends on the liquid velocity which is related to the inlet pressure. Hence, with a decrease of *Re* and *We,* the liquid sheet disturbances decrease and vice versa. Also, the physical liquid properties influence

the atomization. Altieri et al. [19] dealt with the comparison of two different liquids, namely water and oil phase. The oil phase caused an earlier breakup of the sheet and it formed larger droplets.

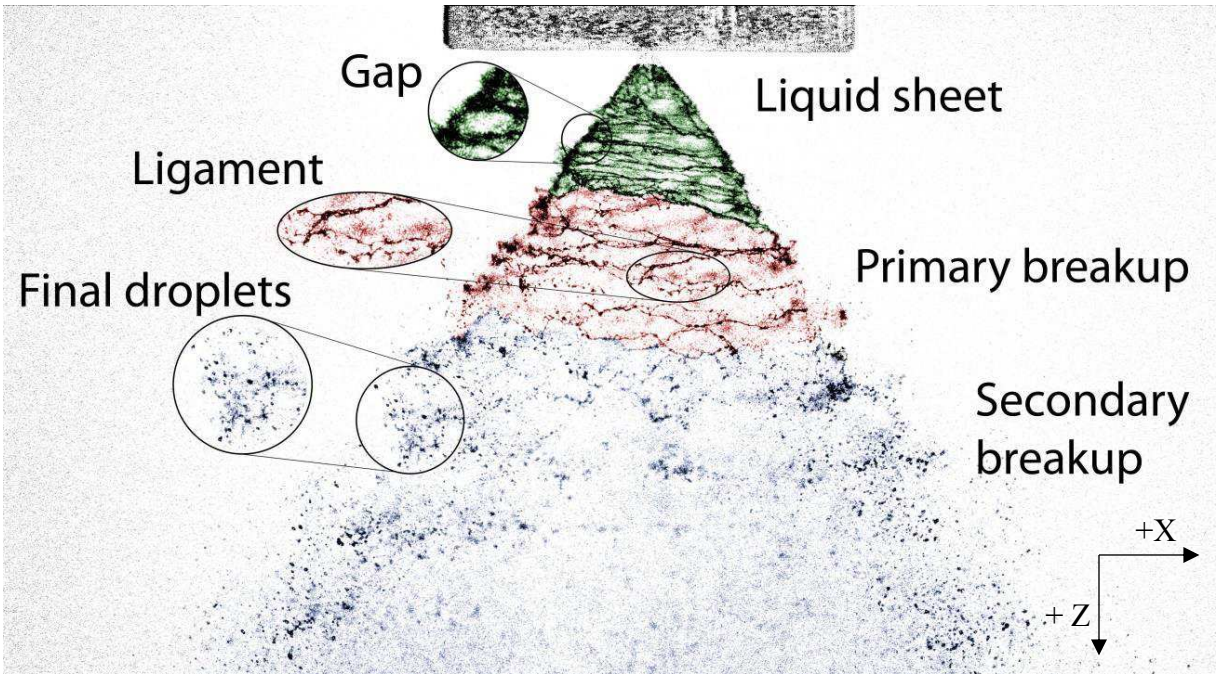

Figure 3-2 Primary and secondary atomization

4 Visualization and optical measurements

Visualization is a process that allows to visualize phenomena that are not visible to the eye. It is applicable to various processes such as flow, heat, sound, chemical kinetics, electromagnetism, etc. [1] The obtained image information serves to a better understanding of the physical nature of the observed phenomena. Besides qualitative it is possible to obtain quantitative information, and therefore the visualization can be ranked among the measuring tools. A detailed study of the visualization methods used in sprays has already been elaborated in the author‘s bachelor thesis [1]. For this reason, only the methods used for the purpose of the present work will be described.

In order to gain the corresponding velocity profiles of the swirling flow inside the atomizer, it is necessary to measure the velocities in two perpendicular directions and their fluctuating components. There are many methods for such measurement, but each method has its limitations, so its choice depends on the type of experiment. For this reason, a study of the possibility of optical measurements as well as visualization was carried out.

Jeng [30] recorded the air core and liquid spray using CCD camera and still photography. Cooper [31] studied waves on the air core liquid interface with the use of high-speed camera and two halogen spotlights. Three distinctive types of waves were detected and subsequently measured by the Laser doppler anemometer (LDA). Hansen [26] in his thesis visualize the air core with the use of a digital camera. He tried to illuminate the interface of the air core and liquid with a laser sheet generated by LDA laser beam expanded by means of an optical probe. However, it was impossible to determine the position of the interface due to reflections on it. Hence the pictures were taken without an artificial light source. Donjat [32] used Laser Induced Fluorescence (LIF) with a laser sheet generated from 448 nm Argon/Krypton laser beam coupled with a CCD camera. Fluorescent dye was injected into the flow to mark out the behavior of an inlet jet. He also used the LDA in backscatter mode to measure the velocity and PIV system which allows getting the instantaneous axial-radial velocity profile. Kenny [33] studied the effect of swirl chamber backpressure on the liquid flow. The air core was captured by the high-speed camera with halogen lamp while the spray features were captured by a digital camera and a high-intensity xenon strobe. The increase in chamber backpressure strongly influenced the internal air core behavior of the swirling flow and it also decreased the spray cone angle and increased the film thickness.

To visualize the internal flow it is necesarry to have some transparent version of the atomizer. Most of the previous mentioned authors used a pleaxiglass material. However, with the use with an inappropriate liquid, the transparency may decrease rapidly. Therefore, it is necessary to choose a liquid whose refractive index is similar to the plexiglas. It is further essential to choose an appropriate visualization method, depending on what exactly will be the subject of the study. A still photography can be used, as in the case of Jeng’s work, but it is limited to just a few static pictures. For a more detailed examination of dynamic phenomena, it is preferable to use a high-speed camera that can capture up to milions of images per second. Such a record can then serve as a video which allows to watch the action in slow motion or backwards, etc. This recording can not be made without sufficient light source, that should be primarily continunous. Therefore, pulse and point lasers are strongly inappropriate.

A sufficient illumination also has to be ensured when the optical measurement of the velocity field. In such a case, the measuring devices exclusively use laser light, both pulse (PIV, LIF) or

continuous (LDA, PDA). Another condition is the presence of seeding particles that follow the flow of the liquid. For more information see subchapter 4.2.

Based on previous information, LDA and high-speed camera were selected for the purpose of this thesis. The selection was also influenced by previous experiences with these devices.

4.1 Laser Doppler Anemometry

Laser Doppler Anemometry (LDA), also known as Laser Doppler Velocimetry (LDV), is an optical method for determining flow velocities in quite different flow situations. It is a non-intrusive measuring technique with good spatial and temporal resolution.

The spatial resolution is given by the size of the measurement volume, which is defined by the intersection of two laser beams. The beams are produced by splitting one laser beam into two parallel beams, that are focused symmetrically by a lens. In the cross area of these two laser beams, an interference pattern can be observed. The interference produce parallel planes of high light intensity, so-called fringes, which are perpendicular to the plane of the drawing, see Figure 4-1 left.

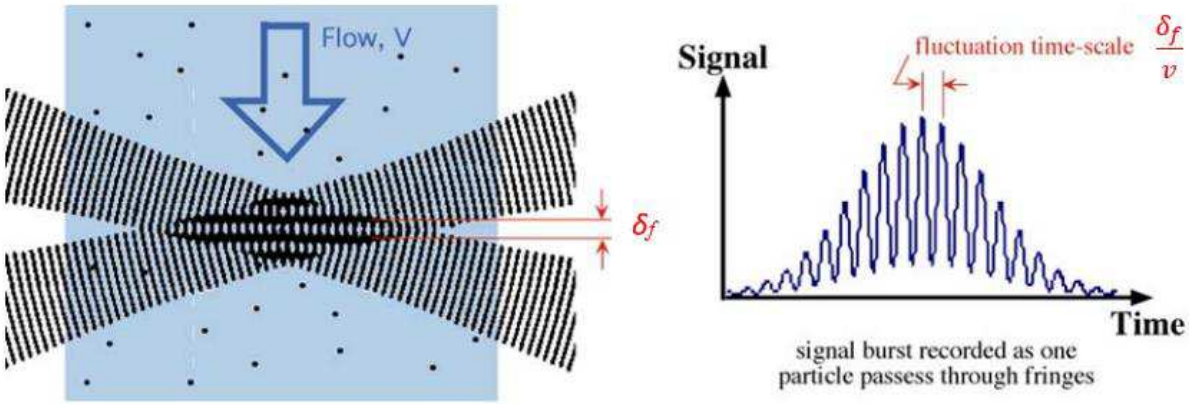

Figure 4-1 Left: Interference fringes. Right: Gausian intensity distribution. [34]

The fringe distance δ_f provide information about the distance traveled by the particle. It depends on the angle between the incident beams θ_b and the wavelength of the laser light λ:

$$\delta_f = \frac{\lambda}{2 \cdot \sin\left(\frac{\theta_b}{2}\right)} \tag{5}$$

Information about the velocity of flow comes from light scattered by particles as they pass through the fringes. The scattered light is collected by a receiver lens and focused on a photo-detector. The result is an oscillating signal, the so-called Doppler signal, that contains the frequency information relating to the velocity to be measured. This signal has a sinusoidal character that reflects the Gaussian intensity distribution in the measuring volume. A better explanation can be given by Figure 4-1, right. When a particle traverses the measurement volume the amplitude of the oscillations increases first and decreases then. [35]

If the fringe distance and the frequency f_D of the Doppler signal are known, it is easy to calculate the velocity of the moving particle in the x-axis (perpendicular to the fringes):

$$v_x = \delta_f \cdot f_D = \frac{\lambda}{2 \cdot \sin\left(\frac{\theta_b}{2}\right)} \cdot f_D \tag{6}$$

The velocity at certain points of the turbulent flow field can be divided into an average mean value v_{x_Mean} and its fluctuation component v_{x_RMS}. The instantaneous velocity will be then equal to the sum of these components:

$$v_x = v_{x\_Mean} + v_{x\_RMS} \tag{7}$$

The subscript 'RMS' stands for *root mean square* velocity given as the standard deviation of the set of "random" velocity fluctuations. A larger v_{x_RMS} indicates a higher level of turbulence and vice versa. [36] Turbulent eddies create fluctuation in velocity. A steady flow would have low turbulence, so $v_x = v_{x\_Mean}$. An unsteady flow would have higher turbulence, so the velocity record includes both a mean and turbulent component. Whether a flow has "low" or "higher" turbulence is given by a Turbulence Intensity (TI), which is a scale characterizing turbulence expressed as a percent. It is defined by the following equation:

$$TI = \frac{v_{x\_RMS}}{v_{x\_Mean}} \cdot 100 \tag{8}$$

According to [37], an idealized flow with absolutely no fluctuations in velocity or direction would have a Turbulence Intensity value of 0%. This idealized case never occurs.

4.2 Seeding particles

The LDA is able to measure only if through the measurement volume passes particle that scatters laser light. If the liquid does not contain sufficient natural seeding, it is necessary to supply it artificially. The choice of the seeding has a significant effect on the resulting measurement accuracy.

Literature [38] sets out the basic requirements:

- able to follow the flow,
- good light scatterers,
- conveniently generated,
- cheap,
- non-toxic, non-corosive, non-abrasive,
- non-volatile, or slow to evaporate,
- chemically inactive,
- clean.

Ideally, they should also have approximately the same density as the fluid itself.

One of the most important factors that can affect the ability to follow the flow is a particle size. In general, small particles better follow the flow and they are better visible in the field of interference fringes, but large particles better scatter the light. Particle size is associated with the Stokes number (*Stk*), dimensionless criteria characterizing the behavior of particles

suspended in a fluid flow. The Stokes number is defined as the ratio of the particle response time (time for changing the velocity of the flow) to the characteristic time of the flow [39]:

$$Stk = \frac{\rho_p C_c d_p^2 \overline{v_{tp}}}{18\mu D} \tag{12}$$

where ρ_p is particle or droplet density, d_p is particle or droplet diameter, $\overline{v_{tp}}$ is the mean tangential velocity of particle or droplet, μ is the air dynamic viscosity, and D is the representative geometric parameter such as swirl chamber diameter. According to Guy [40], the C_c is the Cunningham slip correction factor and it is assumed to be ≈ 1 for the droplet sizes in this case.

A high Stokes numbers ($Stk >> 1$) indicate that the particles are not influenced by the fluid – large particles reflect more light, but their response time is longer than the time the fluid has to act on it and so the particle will pass through the flow without much deflection in its initial trajectory. If the Stokes number is small ($Stk << 1$), the particle motion is tightly coupled to the fluid motion [41] and the particle follows the flow appropriately. The special case is when the Stokes number is about one ($Stk \approx 1$). The particles move towards the edges of the vortex so they cannot follow fluid elements perfectly, however, their paths are altered by fluid fluctuations. These findings have been published by many authors, such as [42,43,44].

5 Experimental setup

Experiments were performed in the Spray laboratory at the Brno University of Technology. Following subchapters describe the experimental apparatus used including the atomizers, the test bench with the fluid supply system, working liquids, Laser Doppler Anemometer and high-speed camera.

5.1 Tested atomizers

The pressure swirl atomizer was tested in its original and scaled transparent version, see the text below.

5.1.1 The origininal atomizer

In this study, a small Simplex and SR atomizer were tested. Their schematic layout and geometric configurations are shown in Figure 5-1. The fuel is fed into the hemispherically shaped swirl chamber through three tangential inlet ports with a rectangular cross-section. The fuel acquires a swirling motion and discharges through a circular exit orifice into the ambient air.

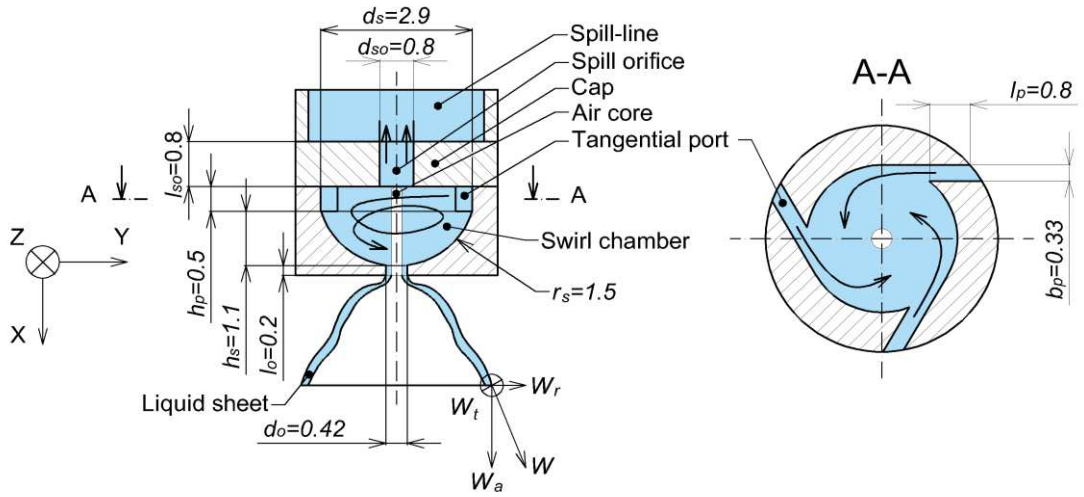

Figure 5-1 Illustration of the original SR atomizer, main dimensions in milimetres. The Simplex atomizer has the same geometry and size, but the spill-line orifice is missing. The transparent atomizer has the same shape, and all dimensions are 10 times larger.

Tab. 5-1 Atomizer dimensions

Nomenclature	Description
b_p	Width of the inlet tangential port
d_o	Diameter of the exit orifice
d_s	Width/diameter of the swirl chamber
d_{so}	Diameter of the spill-line orifice
h_p	Height of the inlet tangential port
h_s	Height of the swirl chamber
l_o	Length of the exit orifice
l_p	Length of the inlet tangential port
l_{so}	Length of the spill-line orifice
r_s	Radius of the swirl chamber

5.1.2 The scaled atomizer

The spray characteristics are strongly linked to the internal flow. For this reason, the transparent version of the original atomizer had to be constructed. However, it was not possible to perform optical measurements inside the atomizer with such small dimensions, therefore the geometrically identical transparent copy in 10:1 was manufactured, see Figure 5-1. It consisted of three parts, each made from Plexiglas. The bottom one with the swirl chamber and the exit orifice, the middle one with three tangential inlet ports and the top one had a plain wall (in case of Simplex atomizer) or included the spill orifice (in case of spill-return atomizer). All three parts were screwed together. To prevent leaking between the interfaces a thin transparent layer of gasket material was used. All the surfaces were ground and polished to achieve transparency for optical measurement.

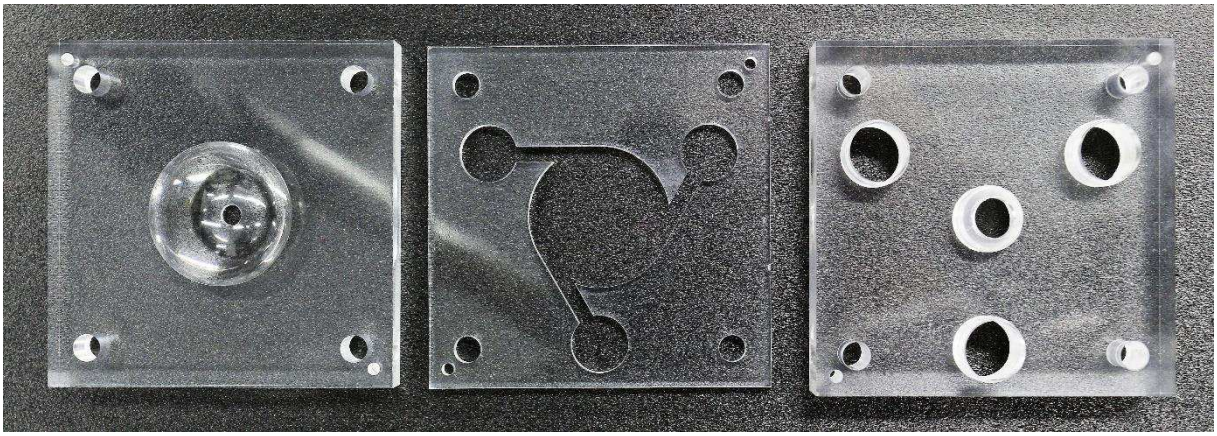

Individual parts of the scaled atomizer

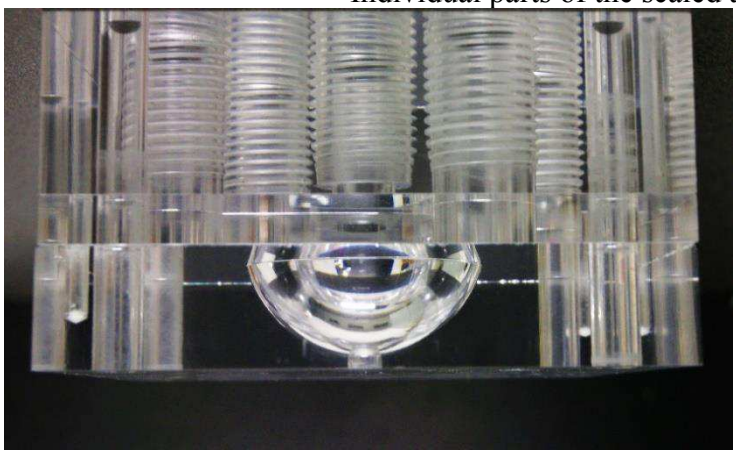

Assembled atomizer, side view

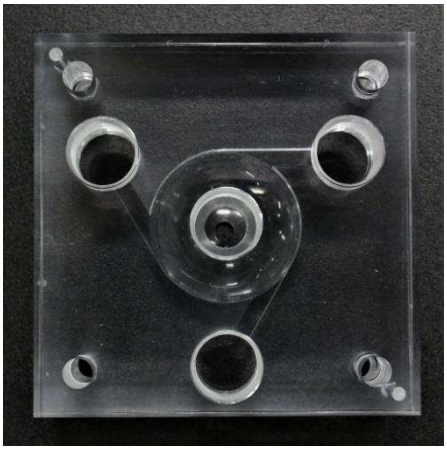

Assembled atomizer, top view

Figure 5-2 The scaled transparent modular atomizer

5.1.3 Flow match

Although the scaled atomizer is ten times larger than the original atomizer, it is necessary to match the flow, so some dimensionless numbers must remain the same as in the original atomizer. Hence a new inlet condition has to be proposed to fulfill these requirements. The following analysis will refer to dimensions shown in Figure 5-1.

- The *Reynolds number* for the scaled model must be maintained to simulate the same internal flow character as in the case of the original atomizer. In the case of the swirl atomizer, the most common definition of *Re* is related to the inlet ports as:

$$Re = \frac{\overline{v_l} \cdot d_p}{\nu_l} \tag{13}$$

where $\overline{v_l}$ is the mean velocity in the inlet ports, calculated as a volumetric flow rate divided by the total cross-section of inlet ports, ν_l is the liquid kinematic viscosity, and d_p is the hydraulic diameter of the inlet ports:

$$d_p = \frac{2 \cdot h_p \cdot b_p}{h_p + b_p} \tag{14}$$

It is not clear at all, what is a critical Reynolds number of a swirling dominant flow, so even if Re = 50,000, it can be assumed as laminar, see Yule and Chinn [45]. Re_c = 2000-3000 applies to the flow in the pipe, but anywhere else it might be different. Therefore, in this work, Re was taken into account in the inlet port where is the laminar flow, so it is assumed that it will persist inside the swirl chamber.

- The *Swirl number* is basically the geometry ratio of the radius of a swirl chamber, an exit orifice, and cross-section of inlets:

$$S_N = \frac{\pi \cdot r_s \cdot r_0}{A_p} \tag{15}$$

where A_p is the total cross-section of the inlet ports. The swirl number has to be the same for the scaled and original atomizers. In the case of this thesis, the swirl number had a value of $S_N = 5{,}99 \times 10^{-12}$ for both atomizers, so the condition was met.

- *The Freude number* shows the effect of gravity in comparison to the energy of the bulk flow:

$$Fr = \frac{Q}{2\pi \cdot (r_o^2 - r_{oac}^2) \cdot \sqrt{r_o \cdot g}} \tag{16}$$

where r_{oac} is the radius of the air core in the exit orifice, and g is gravitational acceleration. It is necessary to keep $Fr >> 1$ to minimize the effect of gravity, as in the case of the original atomizer. The Fr for the lowest pressure used was 6.9, thus the effect of gravity was small.

All the tests were performed at room temperature 20 °C. The main control parameter was the inlet pressure of the original atomizer and consequently, its mass flow rate, from which Re was calculated, see Tab. 5-2. The SR atomizer was evaluated with both the closed spill-line to simulate the maximum injection rate and various *spill-to-feed* (SFR) regimes.

Tab. 5-2 List of operating regimes with their dimensionless numbers

		Original atomizer			Scaled atomizer		
	Re [-]	**Δp [MPa]**	**m_l [kg/h]**	**Fr [-]**	**Δp [kPa]**	**m_l [kg/h]**	**Fr [-]**
Simplex	755	0.5	5.41	137	5	53.8	6.9
Simplex	1021	1	7.31	293	10	73.1	9.3
Simplex	1252	1.5	8.97	359	15	88.2	11.4
SR	1075	0.5	7.70	308	5	69.4	9.8
SR	1431	1	10.25	411	10	93.4	13.0
SR	1731	1.5	12.40	497	15	110.0	15.7
SR, SFR 0.4	1676	1	12.00	481	10	103.0	15.0
SR, SFR 0.8	3756	1	26.90	1078	10	139.4	28.3

5.2 Test bench

Both the original and scaled atomizers were tested under two similarly designed test benches (see Figure 5-3), in order to keep the same conditions. The fuel was pumped from the main tank (1) through a filter (2) by a gear pump or a centrifugal pump (3) to mass flow meter (4), temperature (5) and pressure sensors and control valve (6) into the atomizer (8). The mass flow rate was controlled by varying the pump speed. The spill line was equipped with a pressure sensor (9), a flow meter (10), and a ball valve (11). The spray from the atomizer fall into a collecting container (12) and returned by gravity into the main tank. Fuel vapors were ventilated out by a fan. The atomizer was mounted on a 3D computer controlled traverse system.

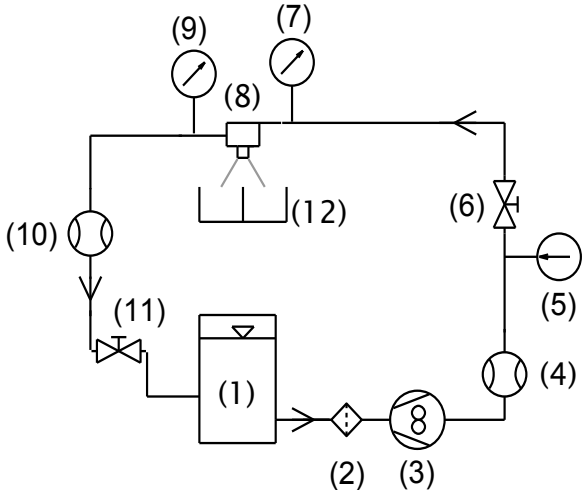

Figure 5-3 Fuel circuit for both original and scaled atomizer

In both cases the following measuring tools were used:

- mass flow meter: For the inlet line: Mass 2100 Di3 Coriolis fitted with a Mass 6000 transmitter (Siemens AG, GE); for the spill line: KOBOLD DOM-S05 (KOBOLD Messring GmbH, GE),
- pressure sensor: DMP 33li (BD SENSORS s.r.o., CZ),
- temperature sensor: PR-13 (OMEGA Engineering, INC., USA).

5.3 Atomized liquids

As already mentioned, this thesis deals with atomizers used in a combustion chamber of the turbojet engine. For combustion is used the aviation fuel Jet A-1 (kerosene) with a density ρ_l = 795 kg/m^3, viscosity μ_l = 0,0016 kg/(m.s) and surface tension σ_l = 0,029 kg/s^2. This was the working liquid for all the tested atomizers. However, when it came to the visualization of the transparent atomizer, it was found out that kerosene is not suitable for this application. The outputs appeared very dark, which made it difficult to assess the fluid behavior inside the atomizer. The reason was different refraction index of kerosene (n = 1.44) and plexiglass (n = 1.49). Therefore, a number of different liquids and mixtures were tested to find the most suitable one. That was the work of my colleague, Bc. Marcel Sapík. In addition, it was necessary to take into account how much liquid damages the atomizer. Eventually, p-Cymene (1-Methyl-4-(propane-2-yl)benzene) was chosen with density ρ_l = 850 kg/m^3, viscosity μ_l = 0,0008 kg/(m.s) and surface tension σ_l = 0,028 kg/s^2. It is a transparent organic compound with refraction index differing from the plexiglass by less than 0.001. It also has a relatively low aggressivity to plexiglass, however, after first measurement hours the atomizer was damaged, especially in the vicinity of bolts and threads, where increased internal tension can be expected.

5.4 LDA setup

When setting up the LDA, it is necessary to pay attention to both hardware and software.

5.4.1 Hardware setup

For the purpose of this thesis the Laser Doppler Anemometer, a 2D FlowExplorer (Dantec Dynamics A/S), and a Dantec BSA F80 signal processor were used. The LDA was configured in a backscatter mode. A built-in diode-pumped solid-state laser generated beams with 660 nm and 785 nm wavelengths. Both the beams were split into two pairs of parallel beams with the power of 30 mW each. The frequency of one beam from each pair was shifted by 80 MHz in order to avoid the ambiguity of the flow direction. A converging transmitting/receiving lens with 150 mm focal length formed an ellipsoidal measurement volume with the size of app. 0.1 × 0.1 × 0.8 mm at the beam crossing point.

The mean velocities of droplets were measured in three cross-sections across the swirl chamber. The axial distances from the top of the swirl chamber were 2.5, 8 and 13 mm for cross-sections a, b, and c respectively (see Figure 5-4), and 50, 38 and 25 measurement points were taken on each cross-section. The distance between two surrounding points was 0.25 mm.

The selected flow tracer particles were SL75 e-spheres with a mean diameter of 45 μm. They are white hollow ceramic microspheres with a bulk density of 450 kg/m^3. Their Stokes number, based on the swirl velocity and diameter of the swirl chamber, was less than 0.01 for each regime, which ensured a sufficiently small flow traceability error.

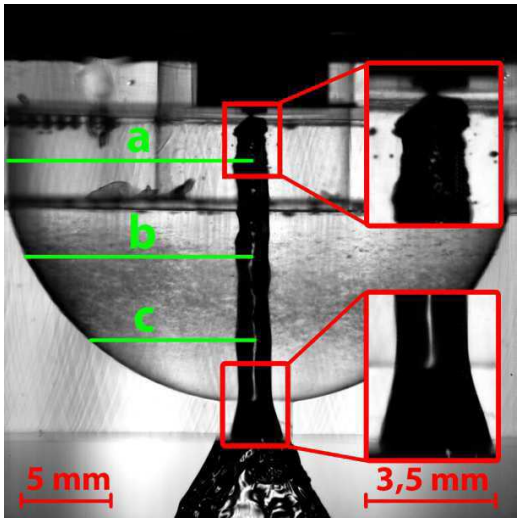

Figure 5-4 LDA measurement positions

5.4.2 Software setup

For all measurements, a BSA Flow Software v5.20 was used to control the data acquisition. The optimal setting results in maximizing the number of detected particles which increases the measurement accuracy. The setup of main parameters that affect the results is as follows:

- **Velocity center and velocity span**: The velocity center determines the mean velocity. The velocity span determines the range of velocity from the center. The center of velocity was set to 2.4 m/s and its span to 4.8 m/s. This range was selected to cover maximum of droplets.
- **A sensitivity of the photo-detectors**: Increase of sensitivity causes a higher data rate[1] but lowers the validation rate[2]. It is, therefore, necessary to find a suitable compromise between them. A sensitivity of 700 V was found to be ideal.
- **Signal gain**: Gain amplifies the signal from photo-detectors. As sensitivity, a higher data rate is accomplished by increasing the signal gain, but the validation rate is decreased. The signal gain was set to 20 dB.

The measurement was limited to 10,000 samples, which leads to a 10-second acquisition duration at each measured point. A repeatability error was less than 4%, based on three consequent measurements [46].

5.4.3 Position and velocity corrections

Due to the different optical path of each laser beam, the differences in refractive index between ambient air, atomizer body and operation liquid cause displacement and distortion of measuring volume, which has to be corrected. In all cases the measuring volume position is corrected as [47]:

$$s_2 = \frac{R_s}{1 + \frac{n_1}{n_2} \cdot \left(\frac{R_s}{n_1 \cdot s_1} - 1 \right)} \tag{9}$$

[1] Data rate – The average number of detected particles per unit of time.
[2] Validation rate - The percentage of valid patterns in the given position.

where s_1 is the virtual distance of the measurement volume from the atomizer wall, s_2 is the real distance of measurement volume, R_s is the radius of the swirl chamber at the measurement plane, n_1 and n_2 are the refractive indices of Plexiglass and kerosene respectively.

It was also necessary to correct the measured velocity, in the case of kerosene. According to Zhang [47], the measured velocity was multiplied by correction coefficient k_{vel} based on the simplified approach as:

- For radial velocity component:

$$k_{vel} = \frac{n_1}{n_2} \tag{10}$$

- For tangential velocity component:

$$k_{vel} = 1 + \left(\frac{n_1}{n_2} - 1\right) \cdot \frac{s_2}{R_s} \tag{11}$$

5.5 High speed camera

A Photron SA-Z high-speed camera was used to document the liquid behavior inside the scaled atomizer and outside of the original atomizer. The atomizers were illuminated by a LED panel in a shadowgraph assembly, when the camera captured the light reflected from the spray, see Figure 5-5. In the case of an internal flow, there were three records obtained at each pressure regime with the use of both liquids. A general record of the entire atomizer body and the other two of the exit orifice and the top of the swirl chamber in close up, see Figure 5-6. The camera frame rate was 20.000 fps for the general image, the resolution was 1024 × 1024 px and a shutter speed was set to 20 μs. The close-up records used a frame rate of 28.000 fps, resolution 768 × 904 px and the shutter speed of 10 μs. In the case of the external flow, the record of spray at each pressure regime was obtained for both working liquids. The camera worked with the frame rate of 96.000 fps, resolution 384 × 432 px and the shutter speed of 25 μs.

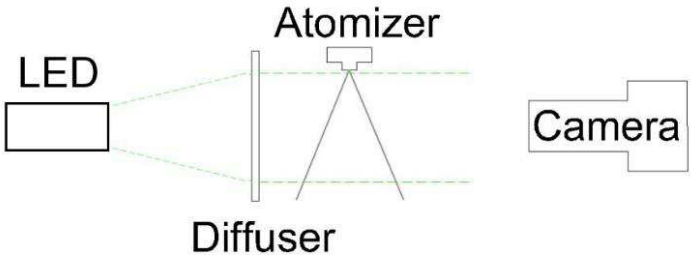

Figure 5-5 Scheme of the shadowgraph techniquie.

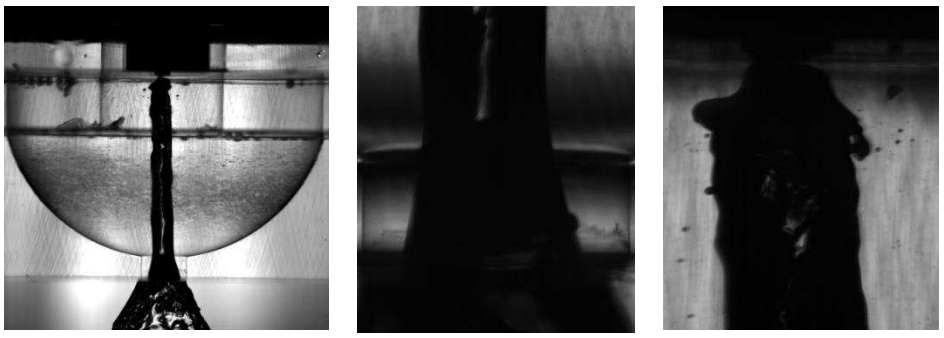

Figure 5-6 From left: the atomizer body, detail of the exit orifice, detail of the swirl chamber top.

6 Results

In the following chapters, the results are presented from both the internal and external flow areas.

6.1 The air core characteristics

In a comparative manner, the high-speed records of the internal flow inside the transparent atomizer with both kerosene and p-Cymene as the working liquid are shown in Figure 6-1. The images of kerosene are darker than the images of p-Cymene, especially in the positions towards the edge of the swirl chamber wall. This is caused by refraction of light at the swirl chamber wall. Due to the small relative curvature of the atomizer center, it is not evident. As it is already mentioned in subchapter 5.3, this problem can be solved using the liquid with the same refractive index as the atomizer body, which is evident from the images of p-Cymene.

The diameter of the air core was measured in four positions – at the input into the tangential ports (1), at the chamber top (2), at the chamber bottom (3), and inside the exit orifice (4), see Figure 6-2, left. In the case of the Simplex atomizer, the air core was stable and fully developed in all tested regimes. It has a cylindrical shape with diameter 2.1 ± 0.03 mm inside the swirl chamber. Inside the exit orifice, the air core has begun to expand to diameter 3.09 ± 0.05 mm, which may be caused due to the change over from the confined to the unconfined nature of the flow with tangential velocity [13]. The same behavior is described in [14,15].

The dimensionless diameter of the air core inside the swirl chamber was $d_a/d_o = 0.47 \pm 0.03$, in the exit orifice $d_a/d_o = 0.72 \pm 0.02$. The air core diameters, and therefore the dimensionless diameters, were almost the same along the entire air core for both liquids. From Figure 6-2, right also implies, that there is no evident correlation to *Re* for the Simplex atomizer. This is in accordance with a theoretical study of Nieuwkamp [48], who also stated that the air core diameter depends only on the atomizer geometry. Those findings were reported by many other authors [14,16,49].

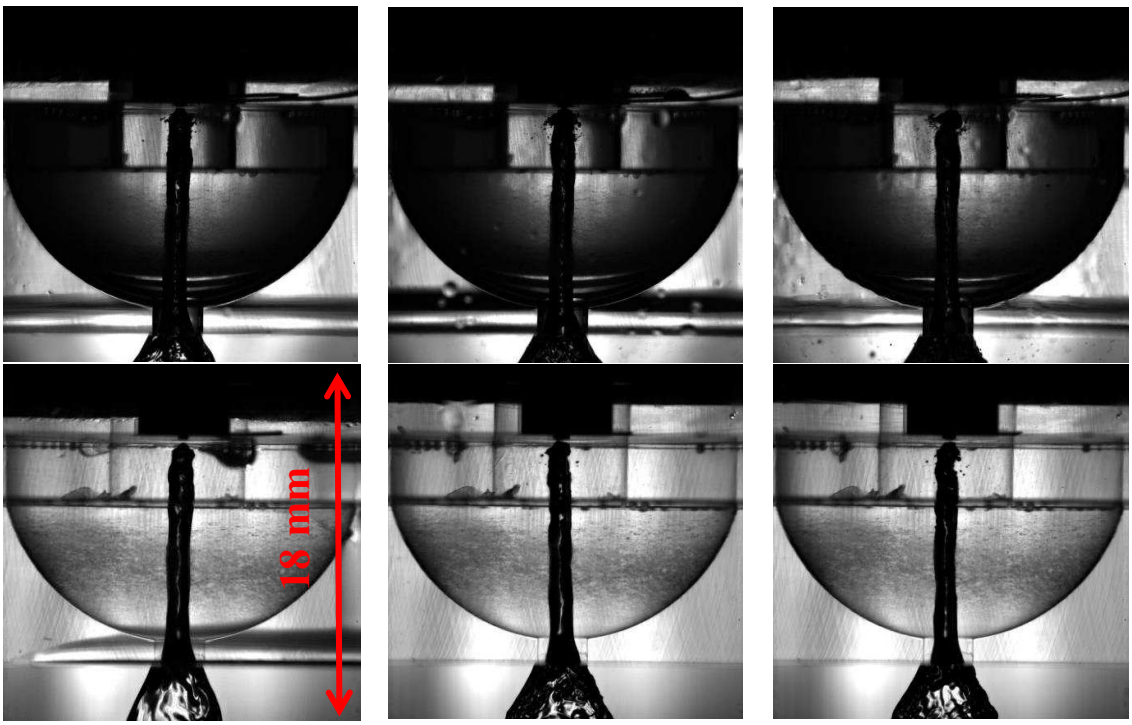

Figure 6-1 Simplex atomizer, Top: Kerosene, Bottom: p-Cymene. From let: equivalent 0.5 MPa (Re = 755), equivalent 1 MPa (Re = 1021), equivalent 1.5 MPa (Re = 1252).

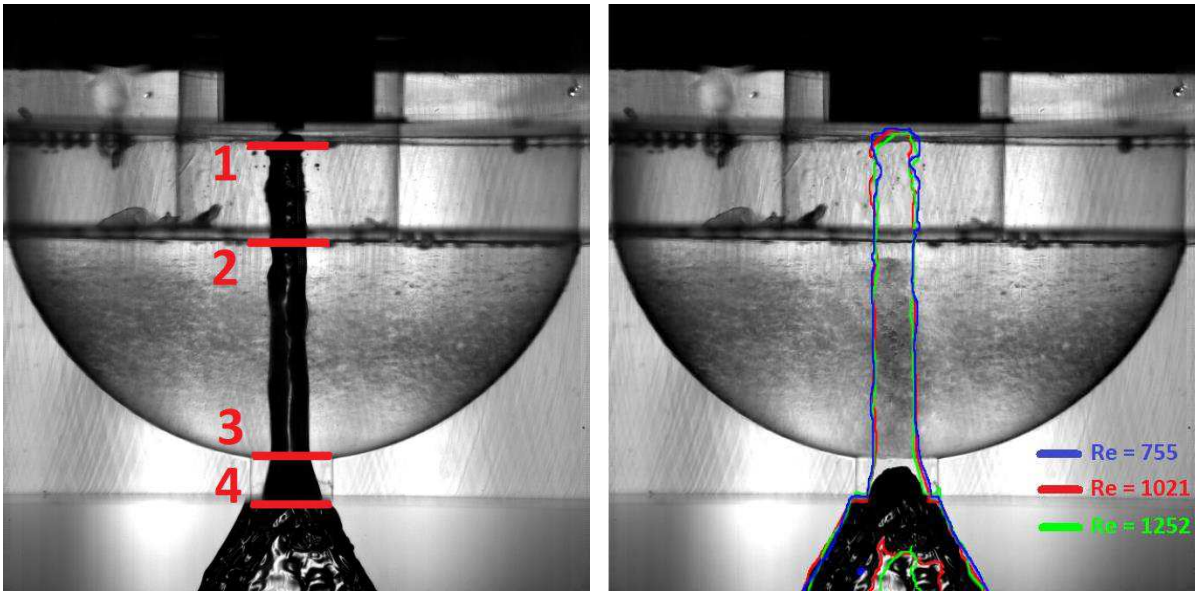

Figure 6-2 Left:Measurement positions of the air core diameter. Right:Influence of Reynolds number on the air core diameter.

The air core fluctuations were observed both in the axial and radial direction at the top of the swirl chamber, see Figure 6-3. These fluctuations are the result of waves on the air core surface. The frequency of the waves $f = 32 \pm 4$ Hz was estimated using the FFT analysis of images for the simplex atomizer with p-Cymene at $Re = 1021$. A similar analysis was reported by Sumer et al. [50] who used a similarly sized atomizer, but with the velocity in the inlet ports approximately ten times higher; they found wave frequencies of $f = 273$ Hz.

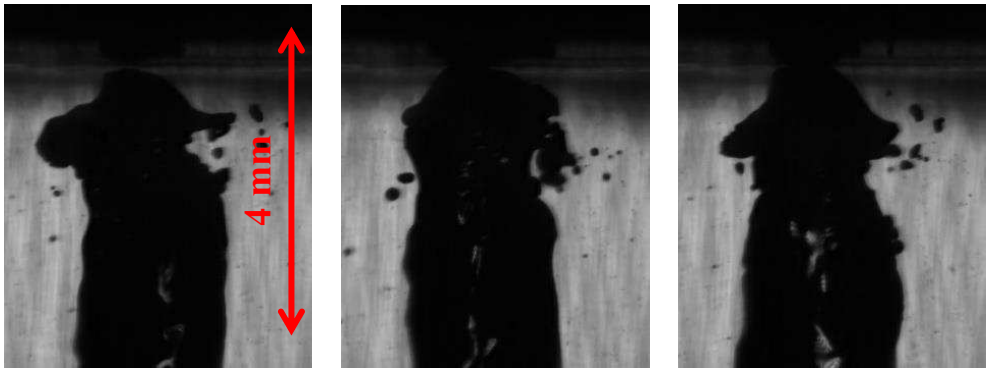

Figure 6-3 Simplex, p-Cymene, Re = 1021. The detail on fluctuating end of the air core.

A different situation occurred in the case of SR atomizer. As it is evident from Figure 6-4, the air core was no longer present in the swirl chamber, only some fragments were visible inside the exit orifice. The air core was unstable with strong fluctuations and it occasionally disappeared. Also, the spray began to fluctuate with a frequency in the range of 10-20 Hz with no evident correlation to the air core behavior. This was observed for all inlet conditions with closed spill-line.

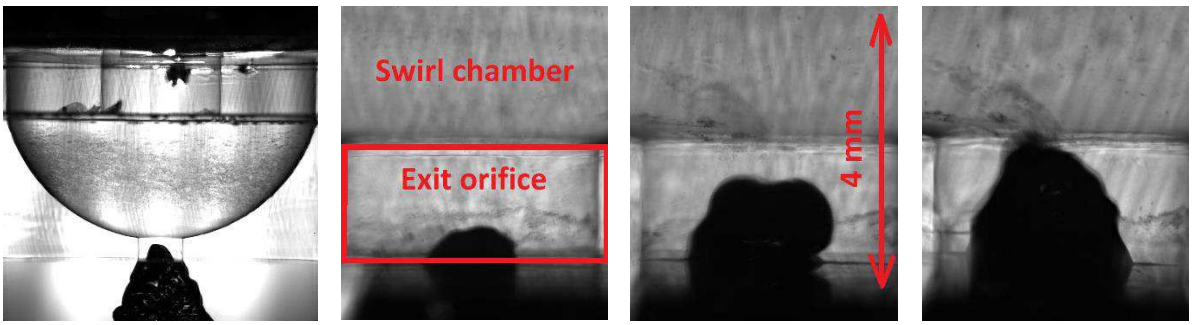

Figure 6-4 SR atomizer. Right: the exit orifice detail., p-Cymene, equivalent 0.5 MPa (Re = 1075), equivalent 1 MPa (Re = 1431), equivalent 1.5 MPa (Re = 1731).

6.1.1 Influence of SFR

When the spill-line is opened, the swirling momentum increases and the flow behavior starts to change. For this purpose, several values of a *spill-to-feed ratio* (SFR) have been investigated, see Figure 6-5. For SFR higher than 0.15 the air core is stable and it is not subjected to decay. The air core occurs only in the area of the exit orifice up to SFR = 0.4, see Figure 6-6, left. After this value is exceeded, the air core is already present in the swirl chamber up to SFR = 0.65. With further increase in SFR, the air core rapidly increase in length and it penetrates through the spill orifice so it is no longer possible to measure its length. The same change is achieved by the air core diameter which significantly increases from SFR = 0.4, see Figure 6-6, right.

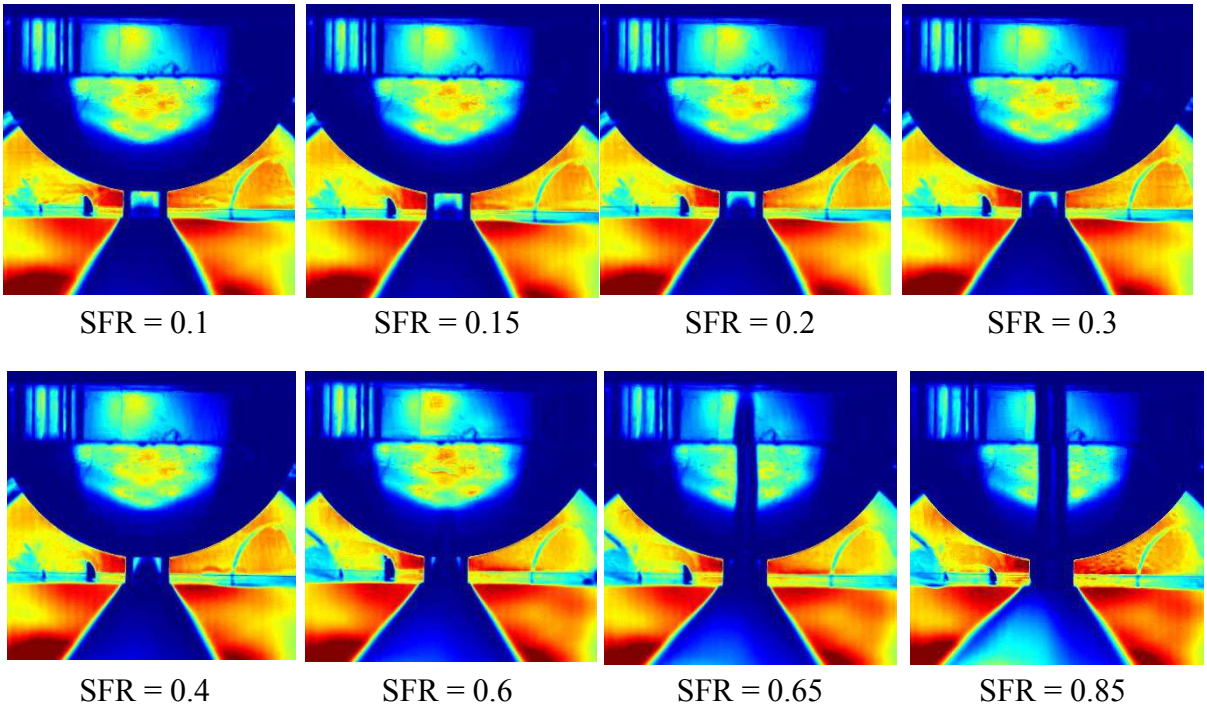

Figure 6-5 Several values of SFR, SR atomizer, kerosene, Re = 1431

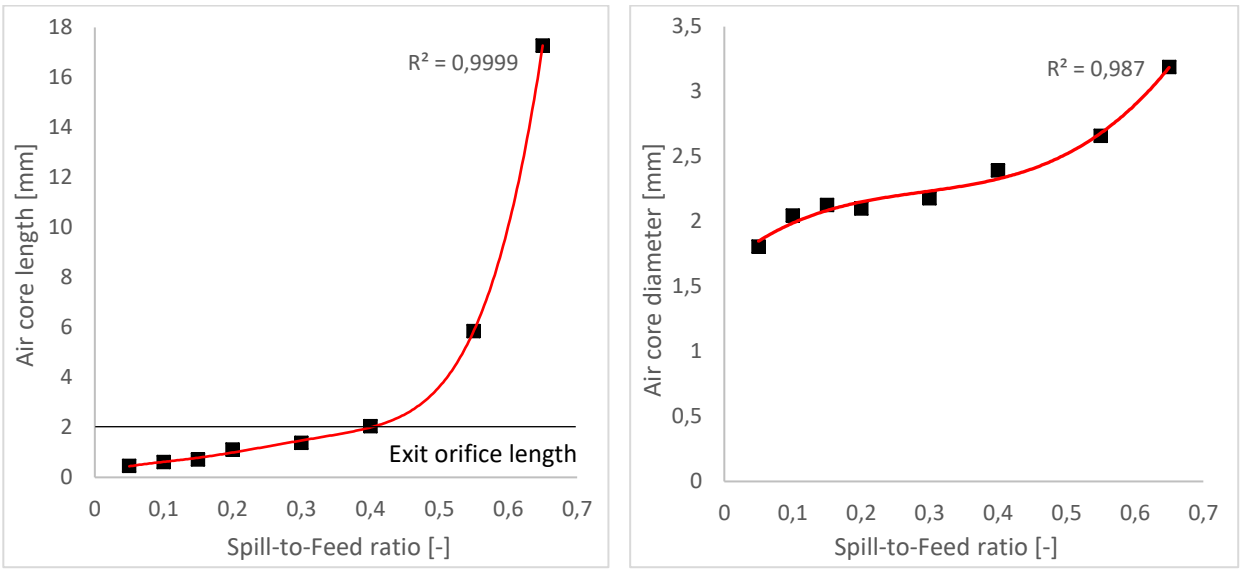

Figure 6-6 The air core length (left) and diameter (right) in dependence on SFR, 1 MPa, kerosene

6.2 Velocity distribution inside the swirl chamber

There is a swirling motion of the liquid inside the atomizer, therefore three velocity components were measured by LDA: axial (v_a), radial (v_r), and tangential (v_t), see Figure 6-7. Their velocity profiles are described below.

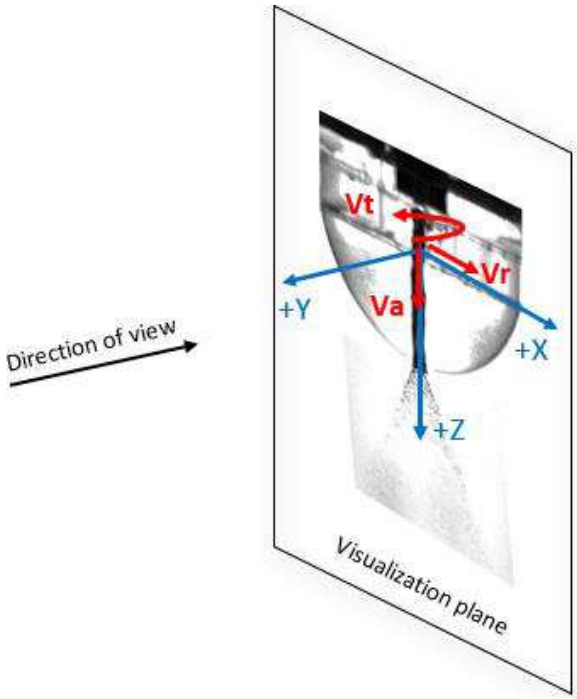

Figure 6-7 Schematic of the velocity distribution inside the swirl chamber

6.2.1 Axial velocity profiles

Although the measurement of axial velocity profiles was carried out, it was not successful. The beams of the measurement volume were probably out of the focus area of the receiving optics, due to the different refractive index of plexiglass. For the next experiments, it might be better to measure this velocity component by Phase Doppler Anemometer (PDA), where the focus can be adjusted.

6.2.2 Radial velocity profiles

When compare Simplex and SR atomizer in Figure 6-8, a similar slope was noticed for each pressure regime. The velocities always reach their maximum near the air core and towards the atomizer wall gradually decreases to zero. However, even the maximum velocities were very small. A similar velocity profile was published by Cooper [24]. According to him, the positive radial velocity near the air core is caused by its expansion as the flow proceeds to the exit orifice. The negative values around the position of 12 mm appear to be due to a small standing wave on the air core.

A 2D numerical simulation was performed by a colleague Ing. Milan Malý using Ansys Fluent 17.2 to compare with the experiment. The setting was made exactly for the identical Simplex version of the original atomizer presented here, with the same operating conditions and working liquids. For more details about the numerical simulation and its setup, an interested reader is referred to [46,51]. Figure 6-9 shows an example of the resulting radial velocity profile for *Re* = 1021. For a better illustration, there is a black line representing the position of 8 mm from the top of the swirl chamber, where the LDA measurement was taken, as in the case of Figure 6-8. It can be noticed that the results of the simulation are ín correlation with the measurement.

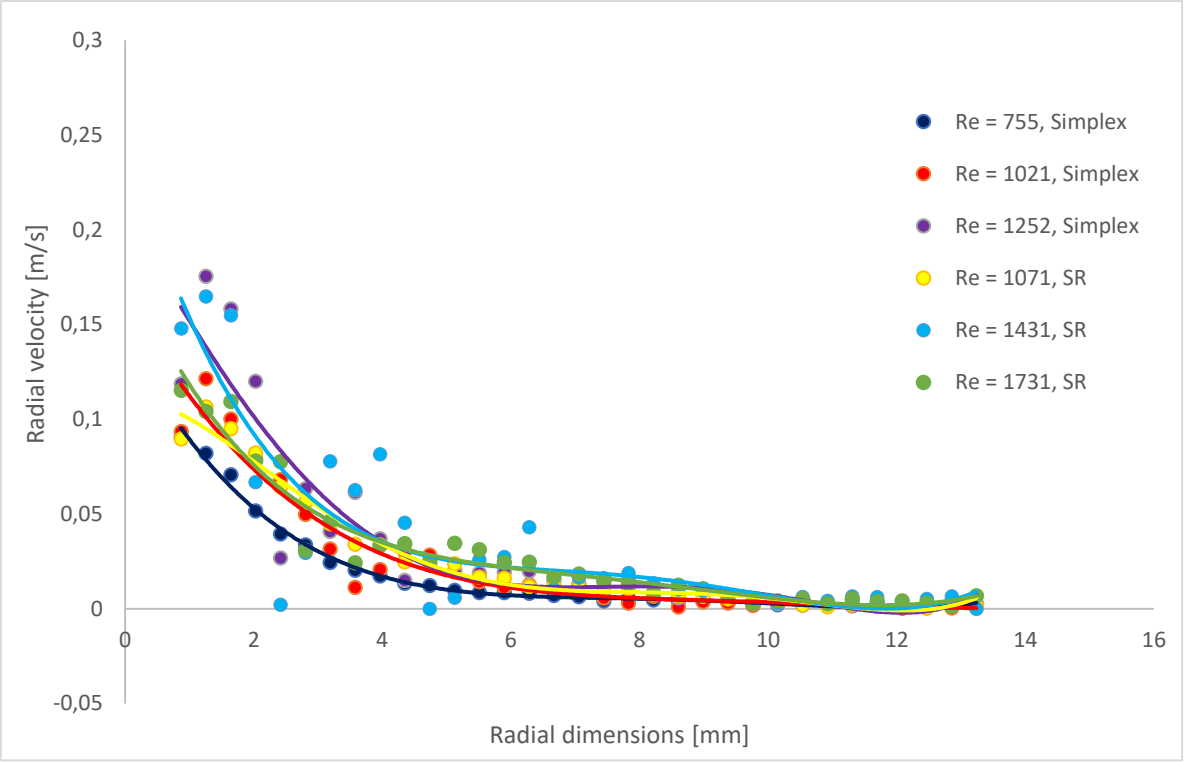

Figure 6-8 Radial velocity profiles, Simplex and SR atomizer, kerosene, Z = 8 mm

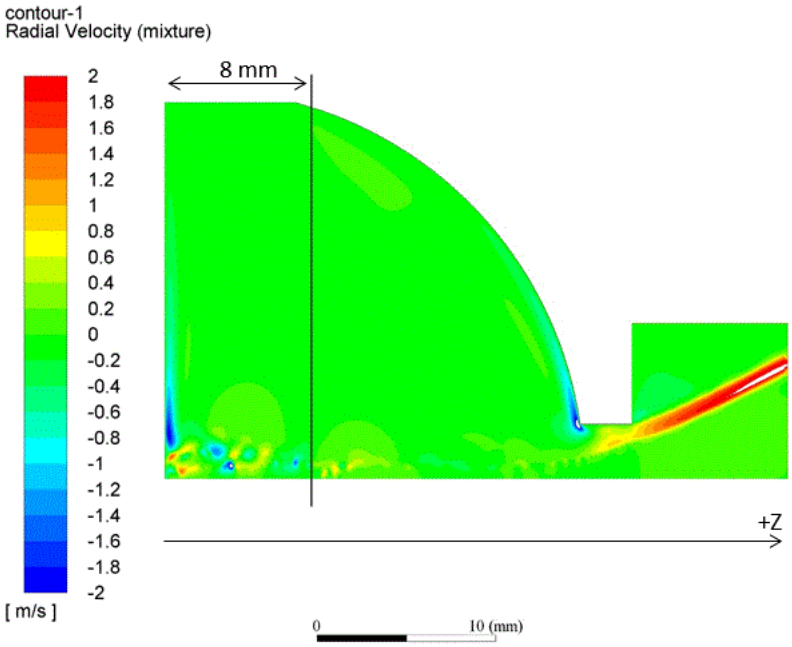

Figure 6-9 Radial velocity distribution obtained from numerical simulation, Simplex atomizer, Re = 1021, kerosene, Z = 8 mm [51]

Figure 6-10 shows a comparison of two working liquids: kerosene and p-Cymene at three axial positions from the top of the swirl chamber. The values of kerosene are higher than those of p-Cymene due to the higher flow rate in order to keep the same *Re*. Again, a similar slope of velocity profiles for both liquids can be noticed. The maximum radial velocity occurs near the air core area and then near the atomizer wall.

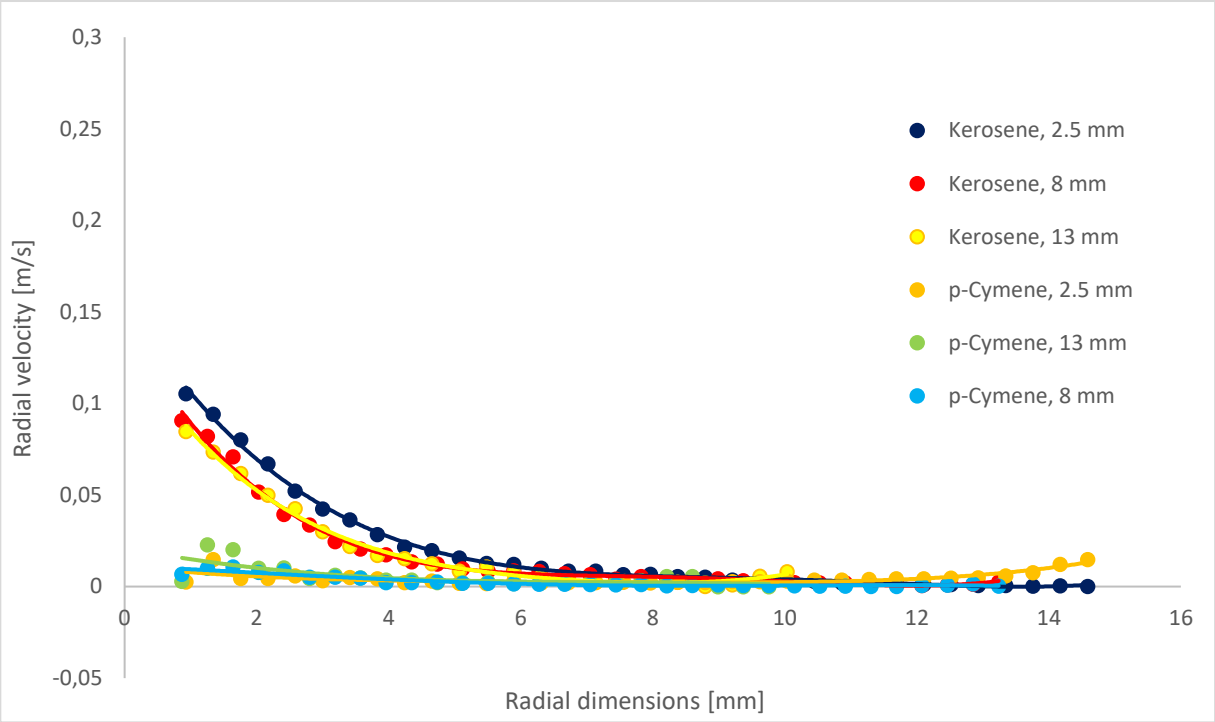

Figure 6-10 Radial velocity profiles, Simplex atomizer, Re = 755

6.2.3 Tangential velocity profiles

The measurement of tangential (swirl) velocity profiles by LDA proved to be different for the Simplex and SR atomizer, see Figure 6-11. The Simplex atomizer had a sharp velocity maximum near the air core interface and a minimum near the swirl chamber wall. The air core behaved like a solid body of the vortex core [23]. These characteristics are similar to a Rankine vortex. On the other hand, the air core is not present in the case of SR atomizer and the whole swirl chamber is filled with the viscous liquid. This causes a decrease in the velocity, so the velocity maximum is lower at similar *Re* values and its peak is flatter.

As in the case of radial velocity, a comparison of the measurement with the numerical simulation is presented here. Figure 6-12 shows the selected tangential velocity profile for the Simplex atomizer working with kerosene at *Re* = 1021, 8 mm from the top of the swirl chamber (see the black line). The simulation shows the same velocity distribution as that measured, which means that the measurement was probably carried out correctly and this velocity profile can be considered credible.

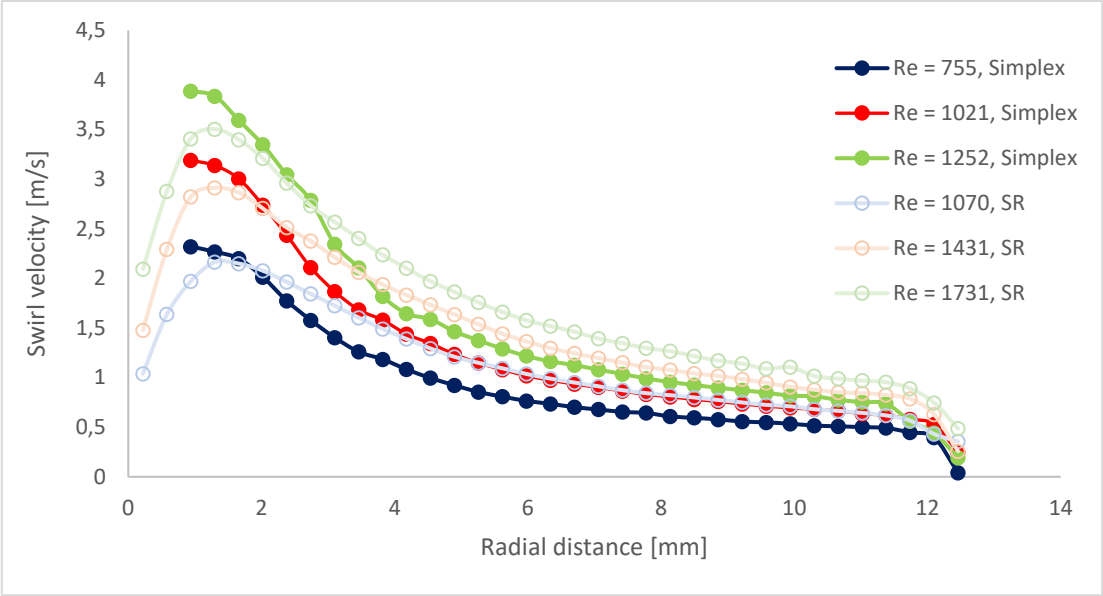

Figure 6-11 Swirl velocity profiles of the Simplex and SR atomizer, kerosene, Z = 8 mm

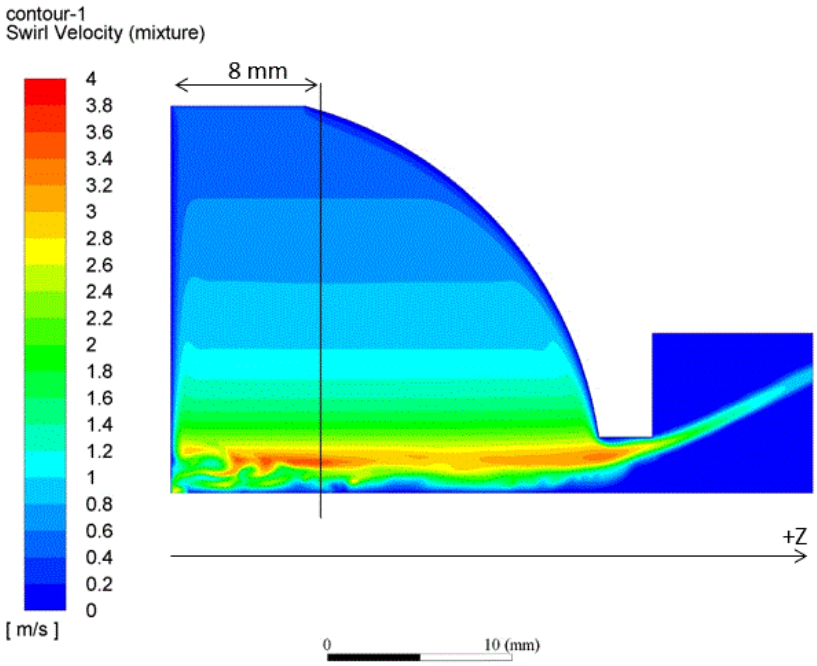

Figure 6-12 Schematic of the tangential velocity distribution obtained from numerical simulation, Simplex atomizer, Re = 1021, kerosene, Z = 8 mm [51]

In addition, the swirl velocity profiles of kerosene and p-Cymene were compared. Figure 6-13 shows the same course of the profiles for both working liquids. Just as was the case with the radial velocity, the values of kerosene are higher than those of p-Cymene due to the higher flow rate in order to keep the same *Re*. There is also evident the independence of the swirl velocity on the axial distance from the top of the swirl chamber.

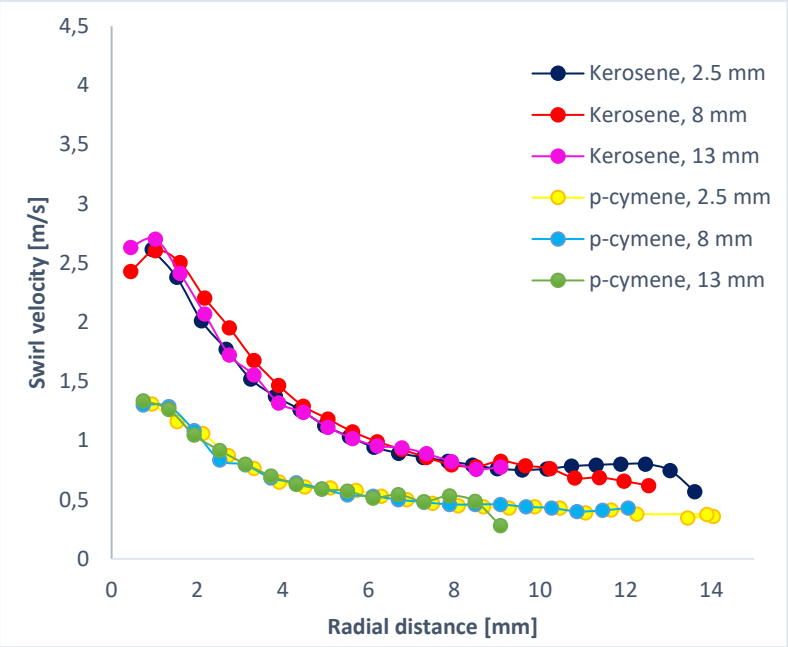

Figure-6-13 Swirl velocity profiles, Simplex atomizer, Re = 755

6.2.4 Fluctuation velocity profiles

In addition to the mean values of the velocity components also the fluctuations were measured. The profiles of both Simplex and SR atomizer showed a similar slope in Figure 6-14 and Figure 6-16. The highest fluctuations appeared in the air core area, where also the highest velocities were measured. Other fluctuations, though smaller, appeared near the wall of the swirl chamber. In radial distance 4-9 mm fluctuations reach the lowest values and can be considered as negligible. It can also be noticed that increasing *Re* increase fluctuations. A similar character can be found in [18,22,23,25]. However, the Simplex atomizer had much stronger fluctuations than SR atomizer near the air core area. This is caused by the absence of the air core inside the SR atomizer. Comparison of both working liquids in Figure 6-15 and Figure 6-17 is consistent with the previous statement. Measurements in different axial positions from the top of the swirl chamber did not bring any significant differences for both liquids. The fluctuation values were almost the same for the radial and tangential velocity component.

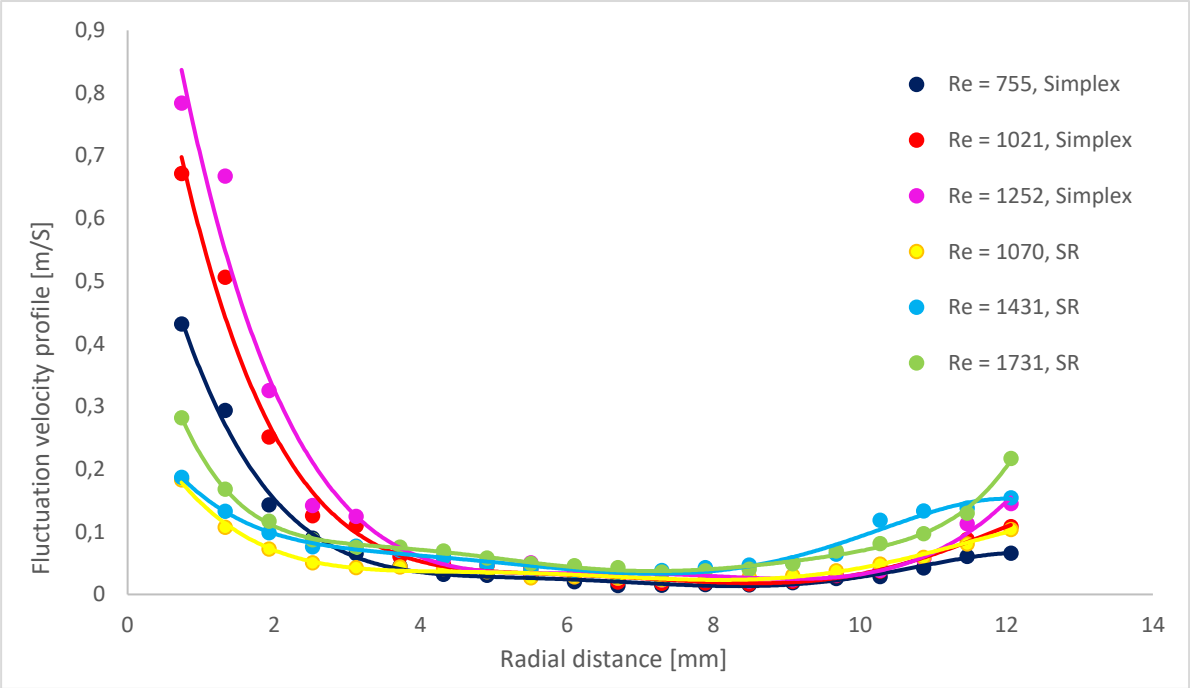

Figure 6-14 Fluctuation profiles of swirl velocity, Simplex atomizer, p-Cymene, Z = 8 mm

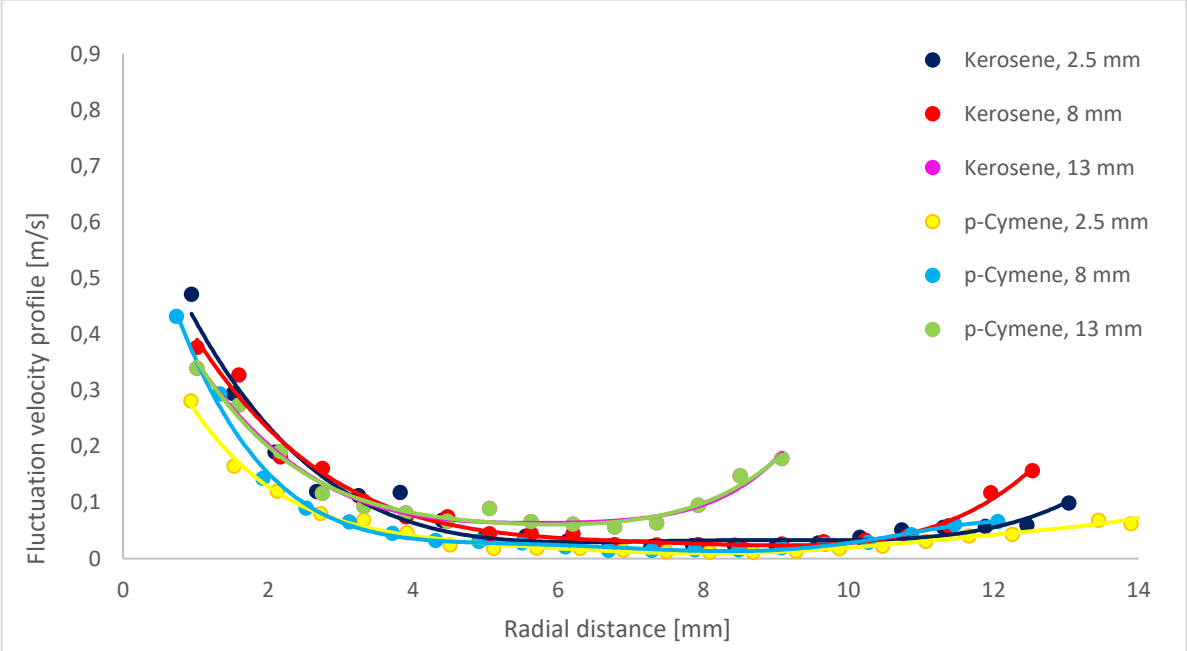

Figure 6-15 Fluctuation profiles of swirl velocity, Simplex atomizer, Re = 755

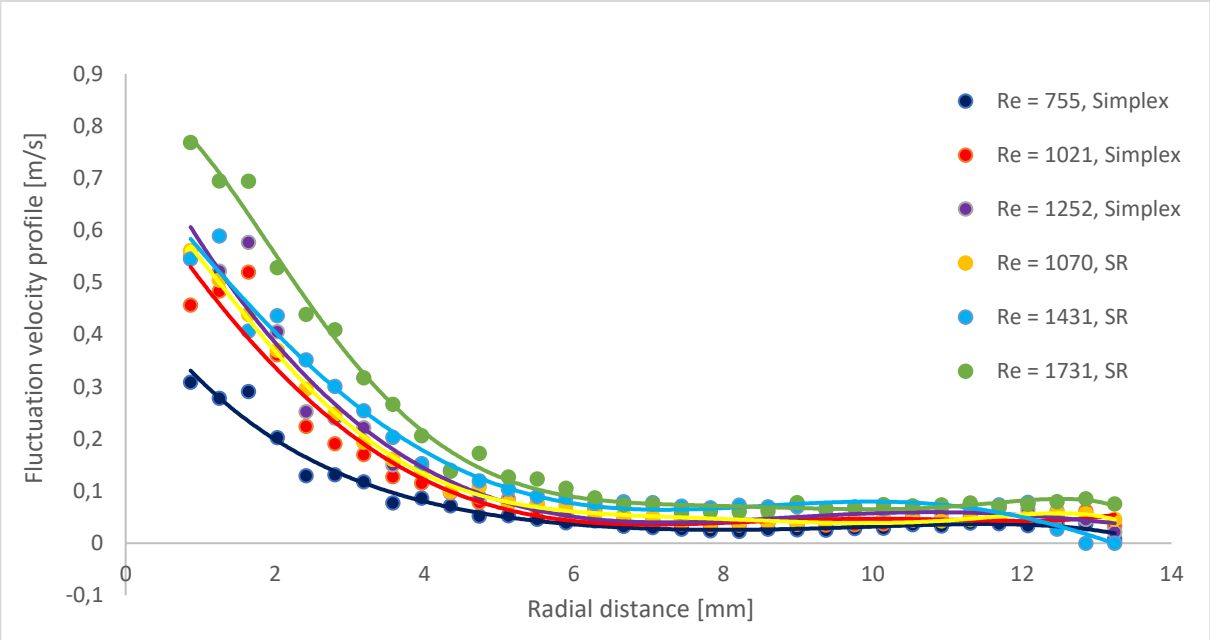

Figure 6-16 Fluctuation profiles of radial velocity, p-Cymene, Z = 8 mm

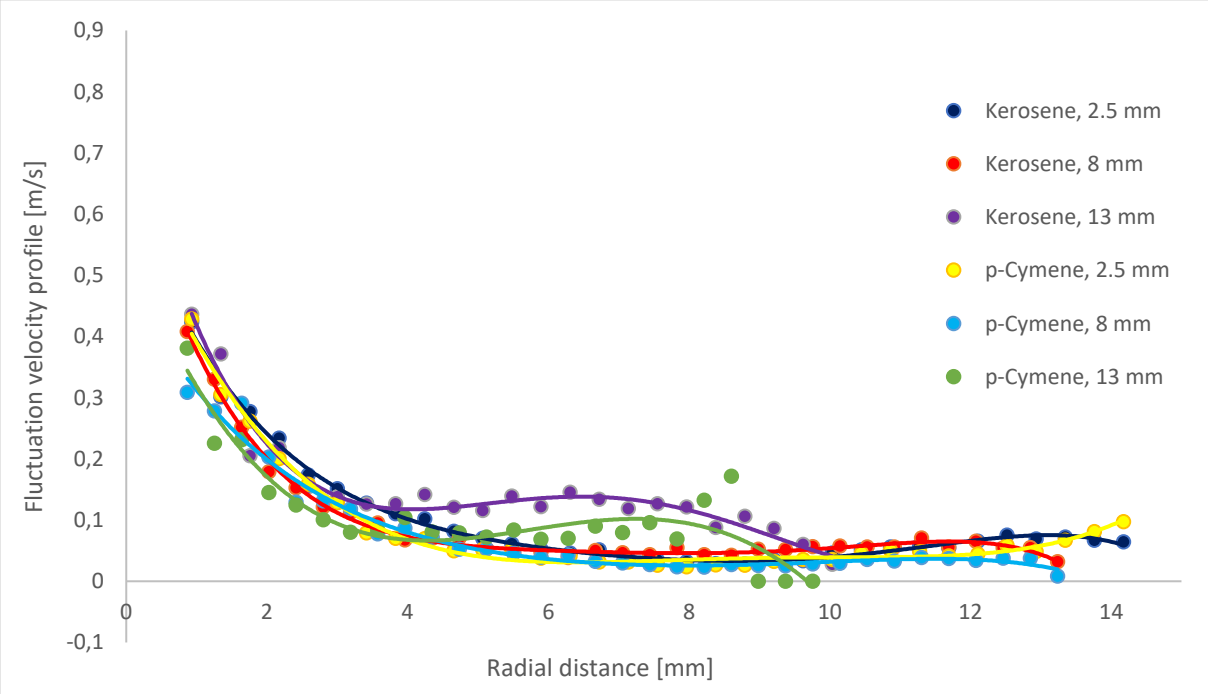

Figure 6-17 Fluctuation profiles of radial velocity, Simplex atomizer, Re = 755

6.2.5 Turbulence intensity

Another expression of velocity fluctuations may be obtained in the form of turbulence intensity (TI). Only the result related to an average tangential velocity is shown for the demonstration. Figure 6-18 shows the dependence of TI on radial distance for both liquids at each pressure regime in the axial distance of 8 mm from the top of the swirl chamber.

In comparison with p-Cymene, kerosene had a little higher TI at the same *Re*. The TI slightly decreased with increasing the inlet velocity (*Re*) in the inlet ports. The greatest increase in TI occurred near the wall of the swirl chamber and close to the air core. However, in these

positions, there are also the largest swirl velocity gradients which can lead to a change of the velocity magnitude throughout the measuring volume and then to false results of TI. The lowest turbulence values were in the center of the swirl chamber, about 3%.

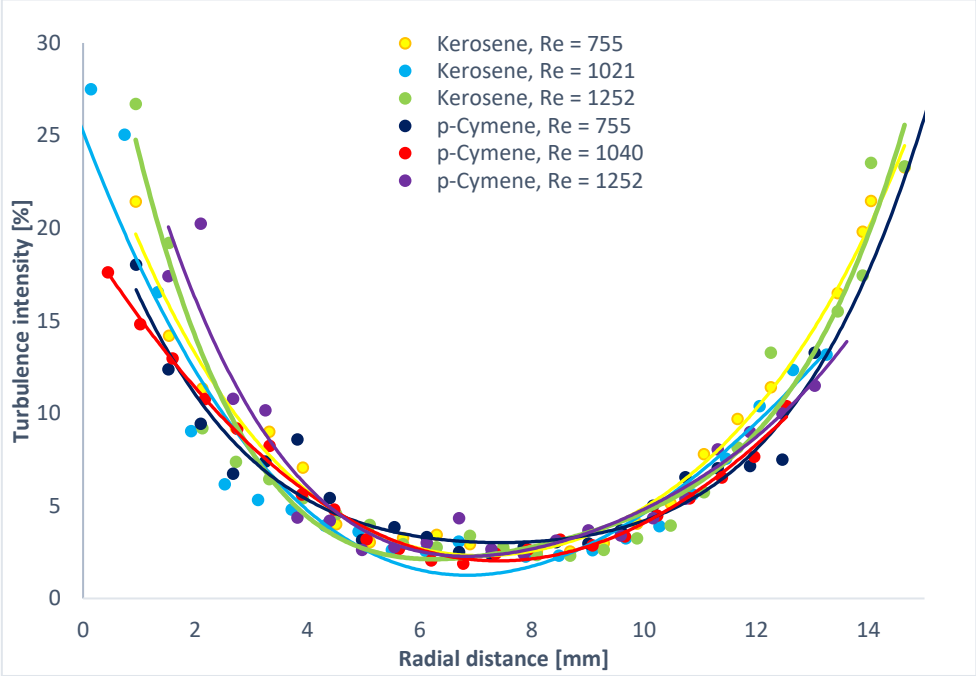

Figure 6-18 Turbulence intensity, Simplex atomizer, Z = 8 mm

6.3 Estimation of the flow field by particle tracking inside the swirl chamber

The present master thesis attempts to deepen an existing knowledge and to estimate the current flow field by means of particle tracking. This can be determined from the high-speed records, for example by PFV software of Photron company, which works well for objects larger and significantly different from the surrounding environment. However, the particles supplied to the fluid are small, not too significant. It is quite easy to lose the particle or to replace it because the software's recognition ability is very small in a non-homogenous environment. Particle tracking is further limited by the record itself, which is usually not long enough to track the entire particle path due to a large amount of data.

For these reasons, a numerical model that can determine the trajectory of a specific particle and the velocity of its movement has been developed in Microsoft Excel. It was based on the assumption that this is a uniformly accelerated circular motion, which means that the change in the trajectory and velocity is proportional to time and the acceleration is constant. Three such movements can be expected inside the atomizer swirl chamber:

1. motion in axial direction – from the top of the swirl chamber to the exit orifice (Z axis),
2. motion in radial direction – a particle radius (X axis),
3. the rotational motion – around the Z axis.

The particles move along the spiraling-helical trajectories, where the coordinates vary app. according to following assumptions:

1. **The motion in axial direction**

The axial direction is given by *Z* coordinate defined as:

$$Z_i = Z_{i-1} + (v_{a,i-1} \cdot (t_i - t_{i-1})) \tag{17}$$

where *t* [s] is a time, (time increment was set to 0.001), and v_a is an axial velocity given as:

$$v_a = \frac{Q}{S_{(t)}} \tag{18}$$

where *Q* [m^3/s] is the discharged flow rate, and $S_{(t)}$ [m^2] is cross-section area of the atomizer at the place where the particle is located at the time *t*.

2. **The motion in the radial direction**

To calculate the coordinates in the *X* and *Y* direction, it is crucial to determine the local radius of the particle:

$$r_{(t)} = \sqrt{\left(\frac{r_{(t0)}^2 - R_{ac(t0)}^2}{R_{(t0)}^2 - R_{ac(t0)}^2} \cdot \left(R_{(t)}^2 - R_{ac(t)}^2\right) + R_{ac(t)}^2\right)} \tag{19}$$

where $r_{(t0)}$ [m] is the initial radius of the particle, R_{ac} [m] is the radius of the air core, *R* [m] is the radius of the atomizer at the place where the particle is located at the time *t*.

3. **The rotational motion**

The rotational motion can be described by the angle of rotation of the particle relative to the zero position (*0,0,R*), [52]:

$$\varphi = (\omega_0 \cdot t) + \varphi_0 + \left(\frac{1}{2} \cdot \varepsilon \cdot t^2\right) \tag{20}$$

where ε is an angular acceleration, φ_0 is an initial angle of rotation, and ω_0 is the initial angular velocity of the particle given as a relation of the initial particle velocity v_0 [m/s] and the radius of the swirl chamber r_s [m]:

$$\omega_0 = \frac{v_0}{r_s^2} \tag{21}$$

The *X* and *Y* coordinates were obtained by converting φ from polar to cartesian coordinates:

$$X = \cos\varphi \cdot r(t) \tag{22}$$

$$Y = \sin\varphi \cdot r(t) \tag{23}$$

The calculated coordinates were plotted, see Figure 6-19. The result was a view of the particle trajectory in the XZ and XY plane. It should be noticed, that values on the axes of the simulated trajectory images (Figure 6-19–6-24) are given in meters.

The values on the axes of the simulated trajetory images are given in milimeters.

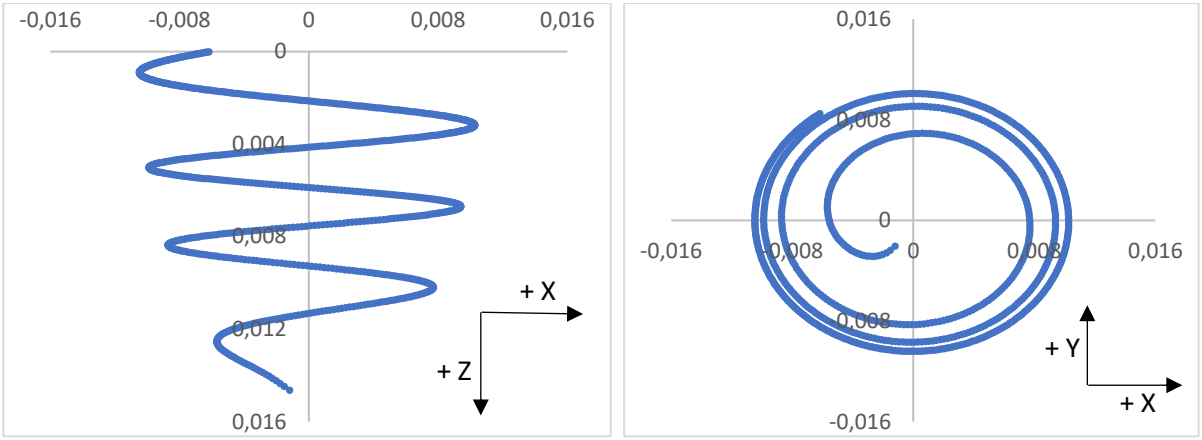

Figure 6-19 Trajectory of a particle obtained from numerical model. Left: XZ plane. Right: XY plane.

This numerical model required real data to be applied. Those were obtained from high-speed records of p-Cymene. For the first tracking, it was necessary to find a particle with the longest record of its trajectory. Planar measurement of the particle coordinates (axial z, and projection of the radial x) was provided during the flow and the axial and transversal coordinates were acquired. The transversal coordinate is a projection of the radial coordinate into the visualization plane. It is further assumed that the projection of the radial coordinates agrees with the radial coordinate at turning points, and that tangential displacement agrees with the observed particle motion when the particle passes the zero meridians (the air core area in the visualization plane). The measured coordinates were converted from pixels to meters, plotted as red dots to a graph of the same size as that from the numerical model, and then overlapped each other, see Figure 6-20.

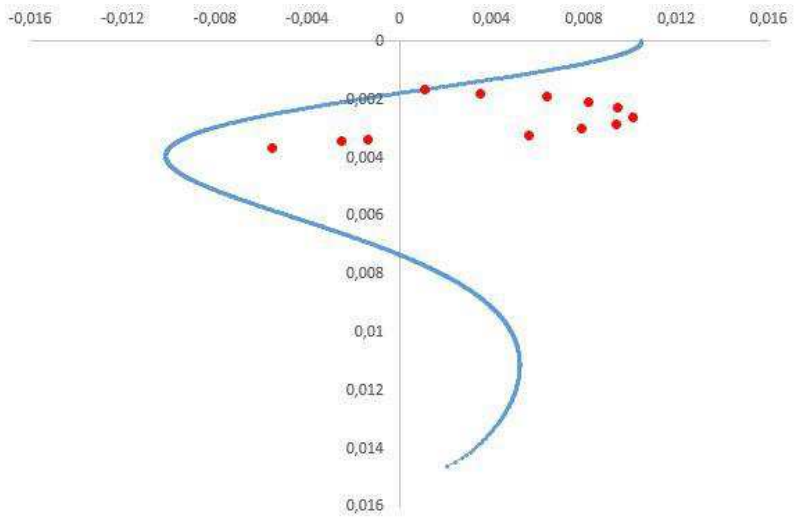

Figure 6-20 Sample overlaped graph of measured particle coordinates (red dots) and calculated trajectory (blue curve), XY plane.

Further adjustments took place only in the numerical model. It has been investigated for which parameters model corresponds to reality. By appropriate alignment of φ_0 and ε, there was a match and the curve overlapped with red dots. It can be stated that the model computes quite accurate at those positions where both curves are overlapped, and the rest of the trajectory is probably also calculated correctly.

At least 80% of the red dots must overlap to say that the calculated trajectory is correctly fitted. The permissible deviation of the red dot from the calculated trajectory is 0.4 mm in the graph.

Thanks to the numerical model also the *y* coordinate (that can not be obtained from a high-speed record) of the particle can be found, see Figure 6-21, right.

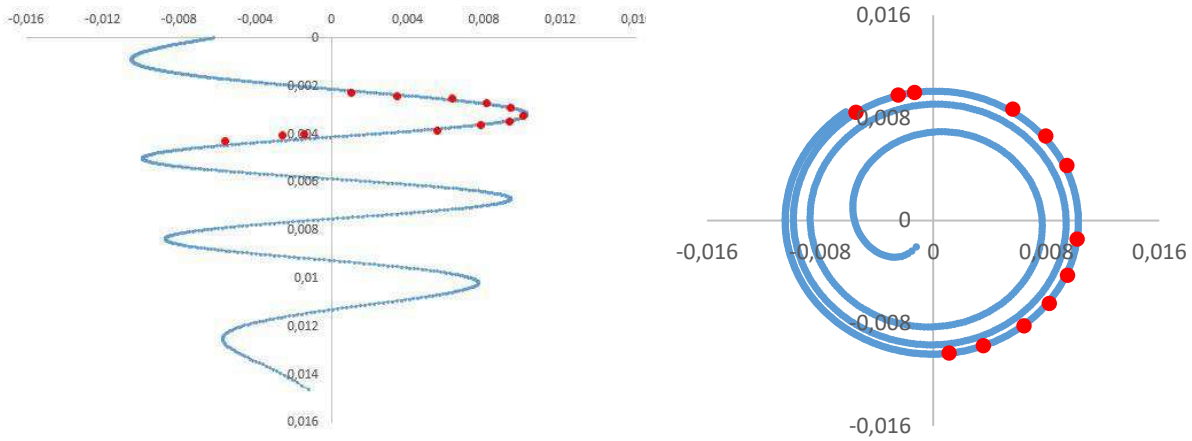

Figure 6-21 Left: The resulting particle trajectory applied to the real data. Right: the position of the particle in the XY plane (see red dots).

6.3.1 The result of the simulated trajectories

The particle tracking was performed from high-speed records of the scaled atomizer with using p-Cymene as a working liquid. The following charts show always three distinct particles circling at different radius for each pressure regime, see Figures 6-22–6-24. The previously assumed swirling motion is obvious.

From the measured tangential velocity profiles by LDA, it was found the highest velocities near the air core and the lowest near the wall of the swirl chamber (see subchapter 6.2). Therefore, it could be assumed that particles rotating at a large radius will move slowly and make only a few turns before leaving the swirl chamber, and particles rotating at a smaller radius (i.e. closer to the air core) will behave exactly the opposite.

However, the numerical model has rebutted this assumption in terms of a number of turns. It can be seen from red and green trajectories in Figure 6-22 and Figure 6-23. The red one represents the particle rotating in the vicinity of the air core, but do fewer turns than the farther green one. A similar case is seen in Figure 6-24, where blue and green curves represent particles circling at almost the same radius. Nevertheless, each one will make a different number of turns. This may be probably due to the fact that each particle has a different initial velocity and enters the swirl chamber at a different angle and direction. This means that the particle can move directly from the inlet port to the center of the swirl chamber, twist a few times and come out, or can rotate many times along the wall before it leaves the atomizer, etc.

It can be noticed, that the trajetories have an ideal shape. This is obvious, because the numerical model does not include the momentum of the particle, forces acting on the particle, etc. Therefore, it is not possible to draw a trajectory with its deflections. For the purpose of this thesis, however, the trajectories can be considered as sufficient.

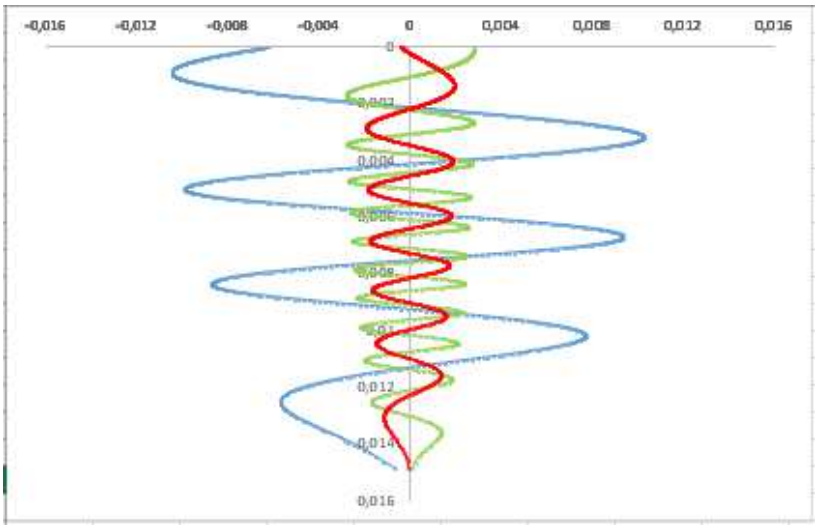

Figure 6-22 Simplex atomizer, p-Cymene, Re = 755

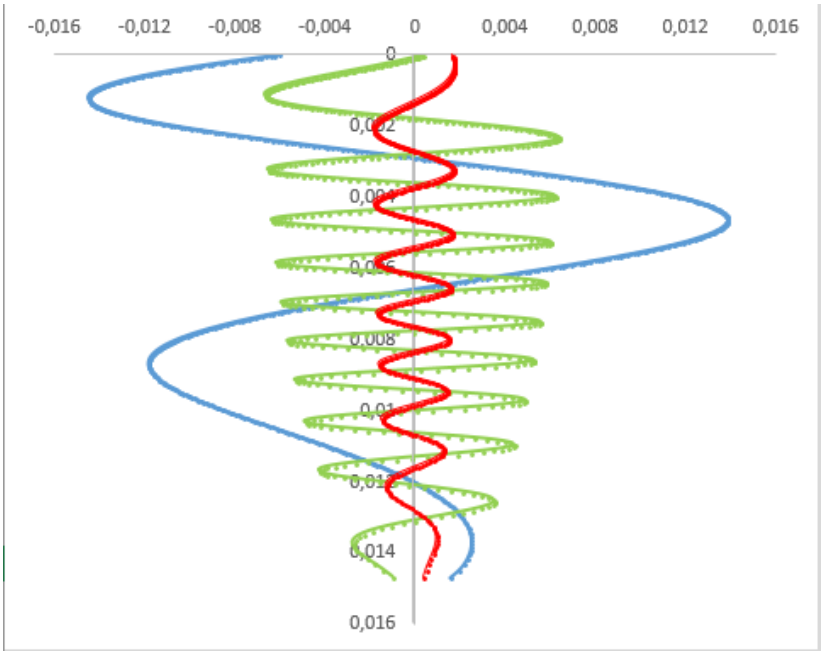

Figure 6-23 Simplex atomizer, p-Cymene, Re = 1021

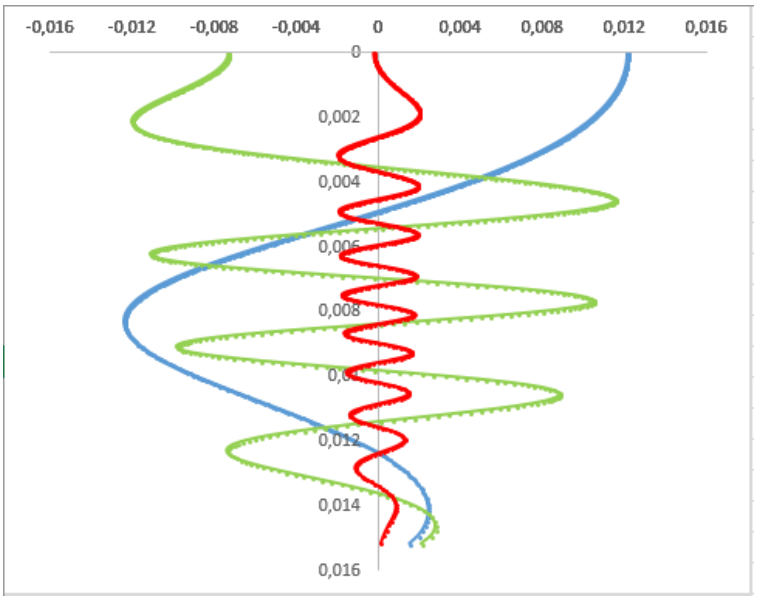

Figure-6-24 Simplex atomizer, p-Cymene, Re = 1252

6.3.2 Velocity profile of the particle

The above mentioned tangential velocity profile measured by LDA was chosen to compare with the velocity profile calculated for specific particles rotating on the largest possible radius (i.e. the blue curves from the previous charts for each pressure regime). The data measured by LDA were used for prescription of the tangential velocity component of each particle. Figure 6-25 shows, that both the measured and calculated profiles almost overlap. The closer the particle get to the air core, the higher is it's velocity, which is in correlation with measurement in the subchapter 6.2. The compared particles have a maximum velocity of 1.1-1.6 m/s. The correction of velocity need not to be made since p-Cymene was used, a liquid with almost the same refractive index as the Plexiglass.

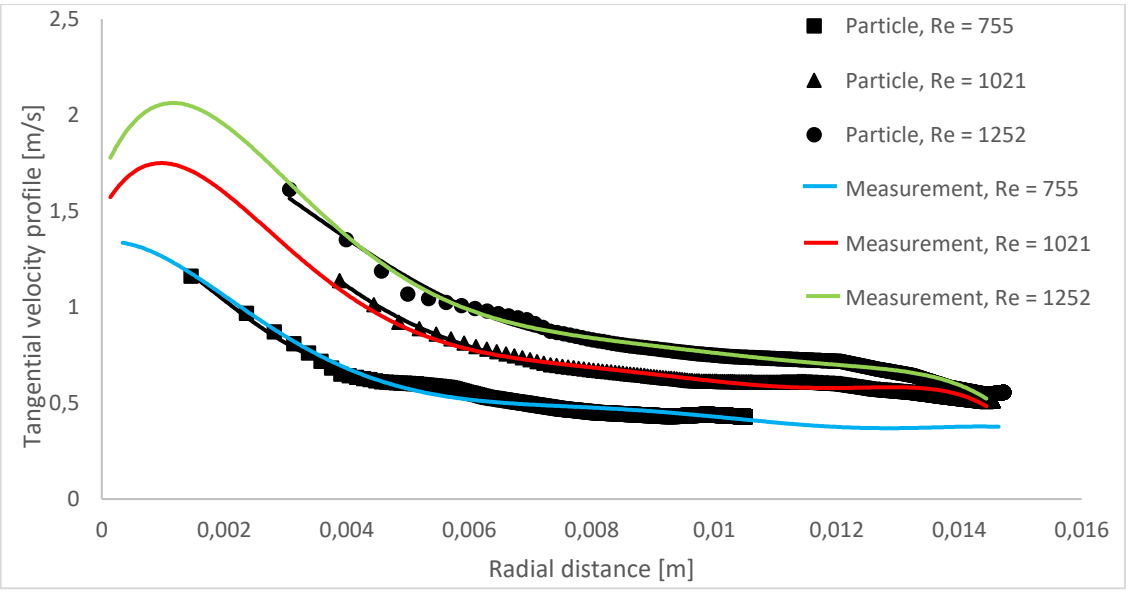

Figure 6-25 Comparison of the measured tangential velocity profile with the calculation for single particles, Simplex atomizer, p-Cymene

6.3.3 Different direction of a particle movement

Thanks to high-speed records it was found that some particles perform the opposite movement, i.e. that they are rotating from the bottom to the top of the swirl chamber. This is a very important feature because it shows the complexity of the flow inside the atomizer. It could be probably caused by the air core that rotates around its axis at high speed, so the flow is similar to the tornado phenomenon, in which is a strong central updraft. Yule et al. [53] reported similar structures inside various atomizers. They further describe that small vortices are formed near the wall of the swirl chamber, which gradually move downwards along the wall, see Figure 6-26. According to Hansen [26], there is no distinct pattern for such a movement, as their size and position are time-dependent. The vortices are known as Taylor-Götler vortices, however, they were not observed from high-speed records in the present thesis. For their documentation it would be appropriate to use, for example, Particle Image Velocimetry.

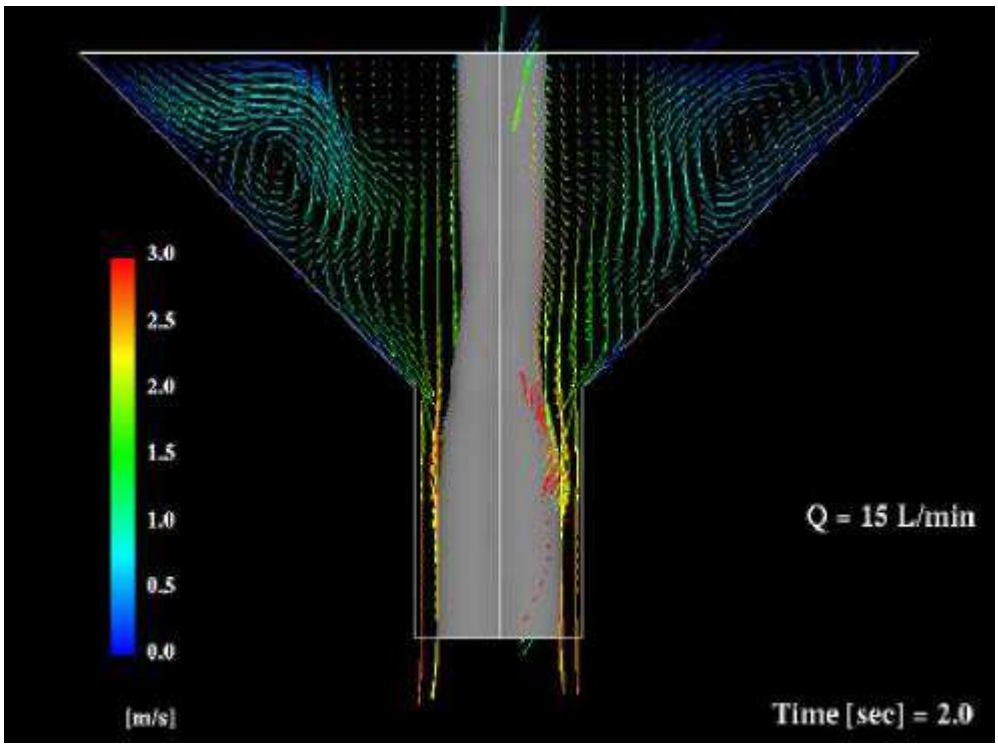

Figure 6-26 The Taylor-Götler vortices inside the swirl chamber ploted by velocity vectors, Hansen [26].

6.4 Liquid discharge

The spray formation and its breakup strongly depend on the internal flow conditions inside the atomizer. The following text summarizes some findings from the study of the resulting spray behaviour, supplemented by calculations of the basic quantities.

The discharge of the liquid can be described by the discharge coefficient, which was calculated using Eq. (1) for both the original and scaled Simplex atomizers. They have the same atomizer constant K, working liquid, and Re, hence the C_D has almost the same values. However, in the case of the SR version, the scaled atomizer featured a noticeably smaller C_D. This behavior was attributed to the diameter of the outflow area behind the spill orifice, which was not sized proportionally in the transparent model according to the original atomizer. This was also observed in [46], where the atomizers of the same design and working conditions were investigated.

In the case of the inviscid flow with no air core, the discharge coefficient could be one [4], i.e. constant and independent on the pressure. Here, however, the viscous flow is taken into account, where the mass flow rate plays a key role. The values of C_D are very low, due to the presence of the air core, which blocks off the central part of the exit orifice. This is an important feature for the formation of the annular liquid sheet. From the following Tab. 6-1 implies, that increase in *Re* leads to a slight decrease in C_D. Generally, increasing the liquid pressure leads to an increase in the velocity inside the swirl chamber; a thinner liquid film is formed in the exit orifice and the air core increase in diameter, which causes a decrease in flow cross-section over the exit orifice, hence the C_D is reduced. This was reported by many authors, such as [17,4,5,14,46].

Tab. 6-1 The reasults of the calculated discharge coefficients, original and scaled atomizer.

		Original	***Scaled***
	Re [-]	**CD** [-]	**CD** [-]
Simplex	755	0.387	0.378
Simplex	1021	0.369	0.366
Simplex	1252	0.365	0.362
SR	1075	0.542	0.483
SR	1431	0.519	0.466
SR	1731	0.510	0.454

The efficiency of the spray production $\eta = \rho_l \cdot v_o^2/2 \cdot \Delta p$ expresses the efficiency of the conversion of inlet potential energy into kinetic energy, and it is related to the exit orifice. The results of η = 0.63-0.71 showed its decrease with inlet pressure. The efficiency of large pressure-swirl atomizers in the study of Yule and Chinn [45] was η = 0.73–0.86, on the contrary Horway and Leuckel [22] introduced η = 0.42–0.66, which applies to different shapes of the swirl chamber. Evidently the size of the atomizer may affect the atomizer efficiency, which explains the different values presented by the authors.

The photographic documentation using high-speed camera was made to observe the formation of the resulting spray and the liquid breakup process. Figure 6-27 shows a spray of the original Simplex atomizer working at three pressure regimes – 0.5, 1 and 1.5 MPa, with the use of kerosene. As it is clear from the author's bachelor thesis [1], the spray can be considered as fully developed for those values.

The liquid emerges from the atomizer exit orifice into the ambient air in the form of a hollow cone liquid sheet. However, the profile is not immediatelly conical, it has a cylindrical shape for a while, which is a remnant of the swirl motion inside the exit orifice. This happens approximately 0.1 mm from the exit orifice. At some small distance downstream it begins to widen and takes the form of a cone. Due to interaction with the ambient air together with fluctuations imposed during internal flow, the liquid sheet begins to oscillate, which produce a wavy structure, see Figure 6-27, left. As the oscillations are amplified, the liquid sheet gradually attenuates with the axial distance from the orifice, and, when the local sheet thickness exceeds a critical value, the liquid film starts to tear into circular ligaments and large droplets. This is the area of the primary breakup discussed in following lines. The liquid structures of primary breakup undergo further disruption into smaller ligaments and then into small single droplets to form the resulting spray.

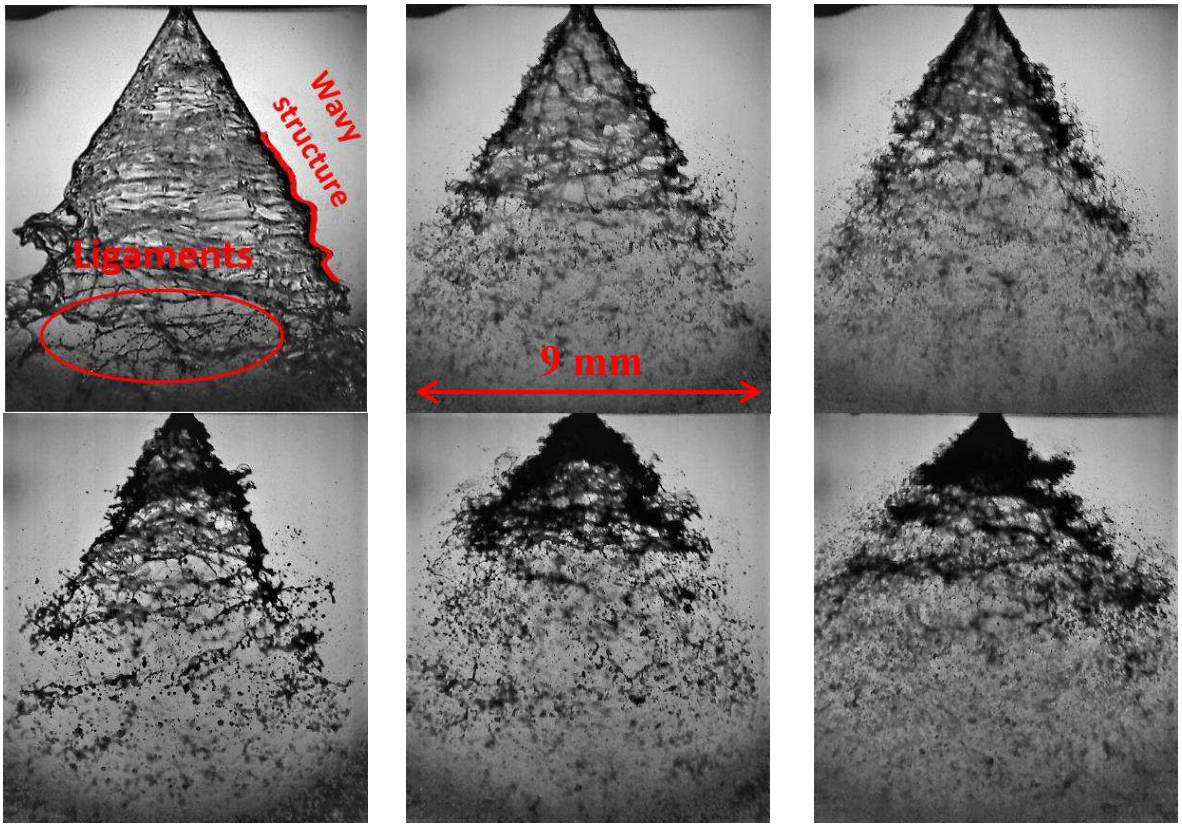

Figure 6-27 High speed images of spray generated by original Simplex atomizer (top), and SR atomizer (down). From left: Δp = 0.5 MPa, 1.0 MPa a 1.5 MPa.

The previous mentioned wavy structure is a typical cause of liquid sheet disintegration in the case of higher discharge velocities (several meters per second). The velocity plays an important role in determining whether the short waves or long waves are responsible for the breakup; according to Senecal et al. [54], this transition can occur at a critical gas Weber number We_{gc} = 27/16. The short waves are dominant for high-speed sheet atomization (when $We_g > We_{gc}$), whereas long waves for the opposite case. When applying this to the present work, the gas Weber number was calculated according to Jedelsky et al. [39] as $We = \rho_g v^2 d/\sigma$, which is similar to the equation (3), with the difference in the density of the gas (air here) with the index *g*. The We_{go} at the exit orifice takes a value of 0.7-1.9. This means, that up to a pressure of 1 MPa the liquid sheet breakup should occur primarily due to the long waves; with a further increase in pressure, the length of the sheet wavy structure gradually reduces, so the short waves begin to be responsible for the breakup. This is consistent with the results of Jedelsky et al. [39], who use the similarly designed atomizer with kerosene working under the same conditions.

The distance from the exit orifice to the first perforation is called „breakup length“, and it should be measured along the edge of the spray. In this case, the measurement of the original atomizer was performed manually from several high-speed images using MB Ruller 4.0, and the mean value was calculated for each pressure regime. In the case of the Simplex atomizer, the sheet began to tear into ligaments at the breakup length of L_b = 2.5-6.3 mm, see Figure 6-28, where the green part of the spray represents the unperforated liquid film for different pressure regimes. There was a rapid decrease in breakup length between 0.5 and 1.5 MPa caused by the increasing shear force with increased injection velocity. The liquid sheet significantly reduced in length in

the case of the SR atomizer, where L_b = 1.7-2.2 mm, and the differences across the pressure range were very small, see Figure 6-29. The similar descending slope was presented by Goodwin [55], however, his measurements were carried out for pressures from 1 to 5 MPa.

The error lines on the measured data show the standard deviation of the data range indicating significant variation for low pressures in comparison with the higher pressures. At 0.5 MPa the breakup process is relatively slow and low aerodynamic forces dominate; even small differences in sheet thickness and structure can strongly affect the change in the breakup length [55], so the formation of the initial holes can move up to 1.3 mm from the mean. When pressure is increased high aerodynamic forces prevail, so small variations of sheet thickness and structure have a relatively small impact on the change of the breakup length. Hence the error lines have lower values.

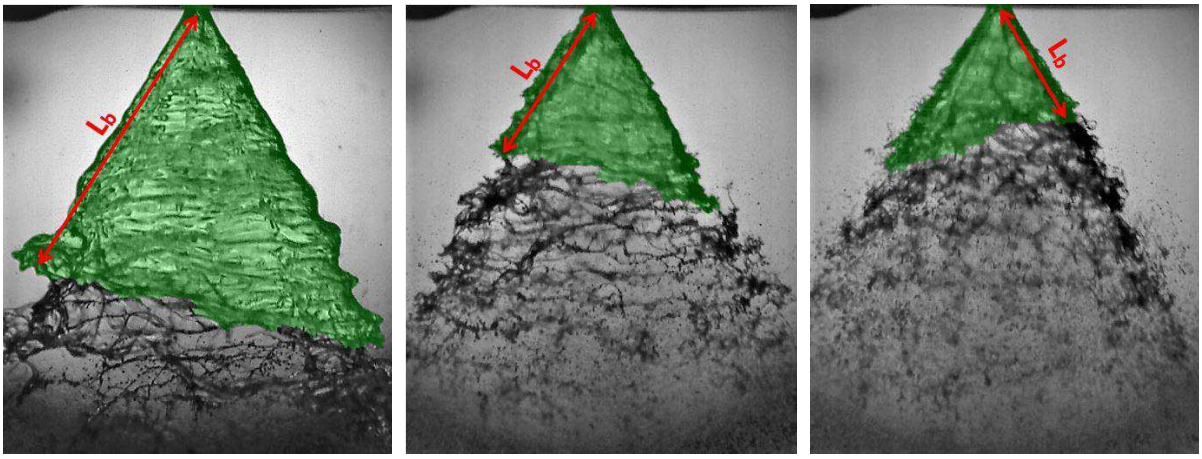

Figure 6-28 Demonstration of the breakup length measurement. original Simplex atomizer, kerosene. From the left: Δp = 0.5 MPa, 1.0 MPa, and 1.5 MPa.

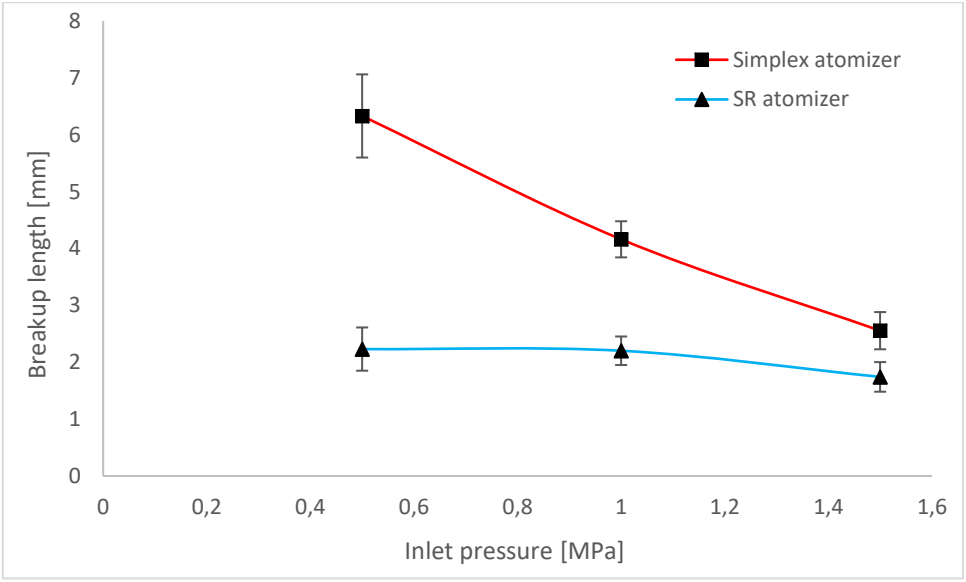

Figure 6-29 Effect of injection pressure on liquid sheet breakup length, original atomizer, kerosene

6.5 Spray cone angle

When the liquid sheet is formed, it is possible to measure the spray cone angle (SCA). The measurement was carried out from the high-speed records by Matlab code based on the Canny edge detector. The result was four values: mean SCA, maximum SCA, minimum SCA, and the

standard mean deviation. In addition, frequencies were calculated in three sections, see yellow, green and blue lines in Figure 6-29. The maximum uncertainty in the spray angle determination is estimated as 2°.

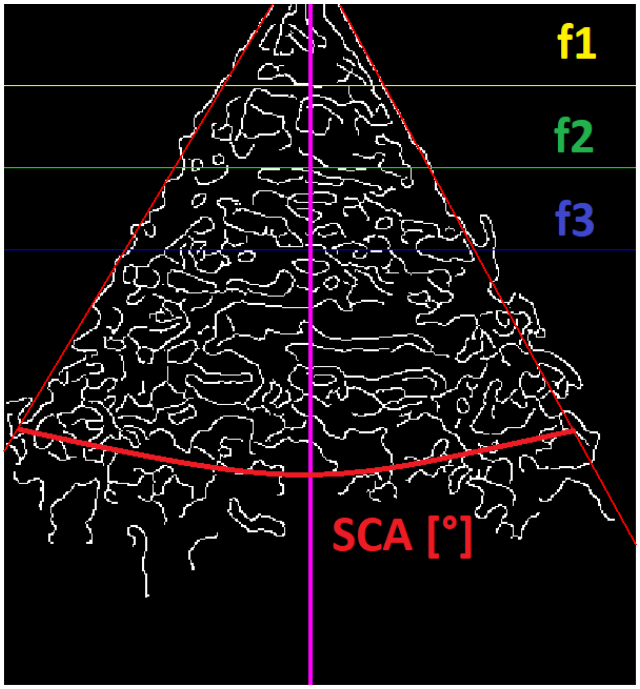

Figure 6-30 Scheme of the SCA measuring

6.5.1 Influence of inlet pressure

The influence of inlet pressure on the SCA has been mentioned in the subchapter 1.2.2. Both the Simplex and the SR type of the original and scaled atomizer are compared in Figure 6-30. Thanks to the fully developed air core in the case of the Simplex atomizer the spray is stable, so the standard mean deviations are at very low values, see Tab. 6-2. Since it is a measured area up to 2 MPa, the SCA variation can be approximated by a straight line law, according to Kutty et al. [56]. As the inlet pressure increases, the SCA widens slowly, which is no more than 2°. On the other hand, the SR atomizer shows strong fluctuations at each pressure regime. The spray is unstable, it behaves unpredictably and forms large drops. Those are very unfavorable conditions for the combustion process, as there is no effective combustion. With an increasing pressure, the SCA expanded by more than 5°. However, although the scaled atomizer has 10 times larger dimensions than the original atomizer, it does not affect the SCA. In both cases, the deviation does not exceed 1%. It can be concluded, that the pressure increase only slightly affects the SCA.

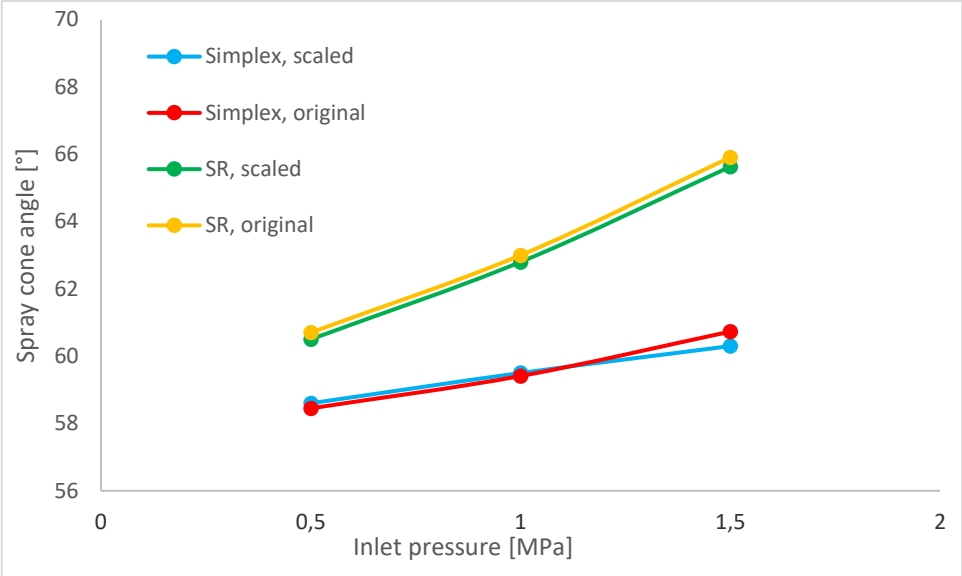

Figure 6-31 Inlfuence of the inlet pressure on the spray cone angle, the Simplex and SR type of the original and scaled atomizers, kerosene

Tab. 6-2 The measured values of SCA and its standard deviations, kerosene

	Original atomizer				**Scaled atomizer**			
	Simplex		**SR**		**Simplex**		**SR**	
Δp [MPa]	**SCA [°]**	**Std [-]**	**SCA [°]**	**Std [-]**	**SCA [°]**	**Std [-]**	**SCA [°]**	**Std [-]**
0.5	58.45	1.51	60.70	7.51	58.60	1.48	60.50	7.60
1.0	59.41	1.95	63.00	8.61	59.50	1.90	62.80	8.53
1.5	60.73	1.91	65.91	9.94	60.30	1.93	65.63	9.89

The SCA can also be determined analytically, however, there are many different relationships listed in the literature. For the purpose of this thesis, three equations were selected and their results were compared with the experiment. The equations are:

Rizk [9]:
$$2\theta = 6 \cdot K^{-0,15} \cdot \left(\frac{\Delta p \cdot d_o^2 \cdot \rho}{\mu^2}\right)^{0,11} \tag{26}$$

Taylor [7]:
$$\tan\theta = \frac{2 \cdot C_D}{\sqrt{K^2 \cdot (1+S)^2 - 4 \cdot C_D^2}} \tag{27}$$

Lefebvre [3]:
$$2\theta = 16.2 \cdot \left(\frac{A_i}{d_s \cdot d_o}\right)^{-0,39} \cdot d_o^{1,13} \cdot \mu^{-0,9} \cdot \Delta p^{0,39} \tag{28}$$

where $K = A_p/\pi R r_o$ is an atomizer constant, C_D is discharge coefficient, and $S = r_{oac}/r_o$ is dimensionless air core radius in the exit orifice.

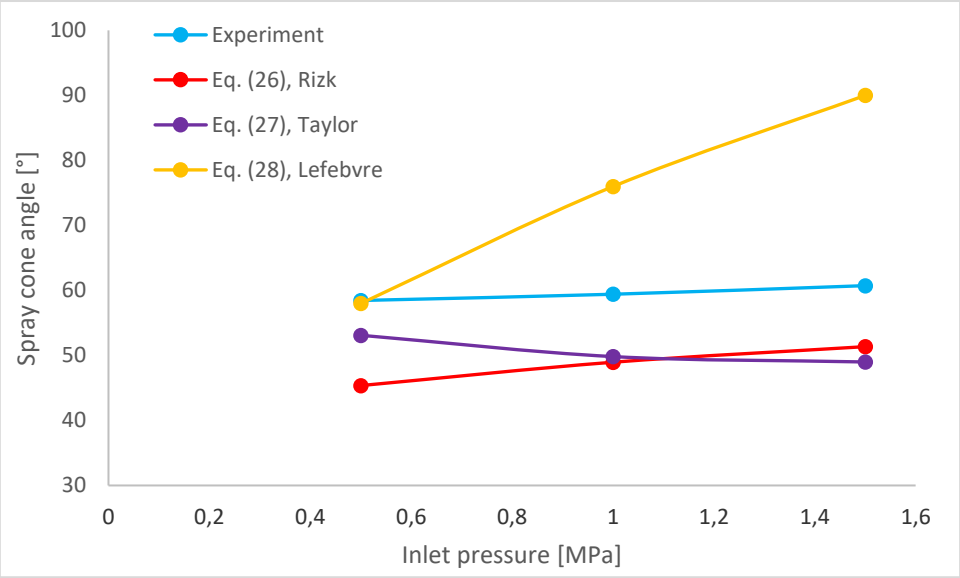

Figure 6-32 Comparison of analytics and experiment. Simplex atomizer of original type, kerosene.

Figure 6-32 shows a chart of three different expressions for SCA plotted against the inlet pressure. All the expressions for SCA are based on conditions in the exit orifice, even so, a significant difference can be seen. Eq. (28) is the most different from the experiment; it is greatly influenced by the inlet pressure, causing a sharp increase in the SCA, up to 30°. Eq. (27) provides somewhat better results, although considerably lower than those measured. It also shows, that the SCA decrease with increasing inlet pressure, which is not right. Obviously, the last Eq. (26) is the closest to reality; the SCA slightly increase with pressure. However, the values are up to 15° lower than the measured ones. It follows from the previous, that the calculation of the SCA is not a very accurate way, but at least it helps to determine the range in which the atomizer can work. For this purpose only Eq. (26) can be recommended, because it was derived directly for kerosene.

6.5.2 Influence of SFR

Stability of the air core influences the stability of the spray. Consequently, the dependence of the SCA at various SFRs was investigated for SR atomizer, see Figure 6-33. Up to SFR = 0.15 spray strongly fluctuates and the standard mean deviation of SCA has high values, see error lines. The fluctuations are reduced with a further increase in SFR. However, at high values of SFR when the injection flow rate is very low, the fluctuations become stronger again. The standard mean deviation of SCA to the SR atomizer at SFR = 0.3 – 0.4 is approximately equal as well as to the stable Simplex atomizer. Therefore, even if the air core is not fully developed (in the case of SR atomizer), it is not necessary to provide a fully developed air core across the whole swirl chamber to ensure a stable spray.

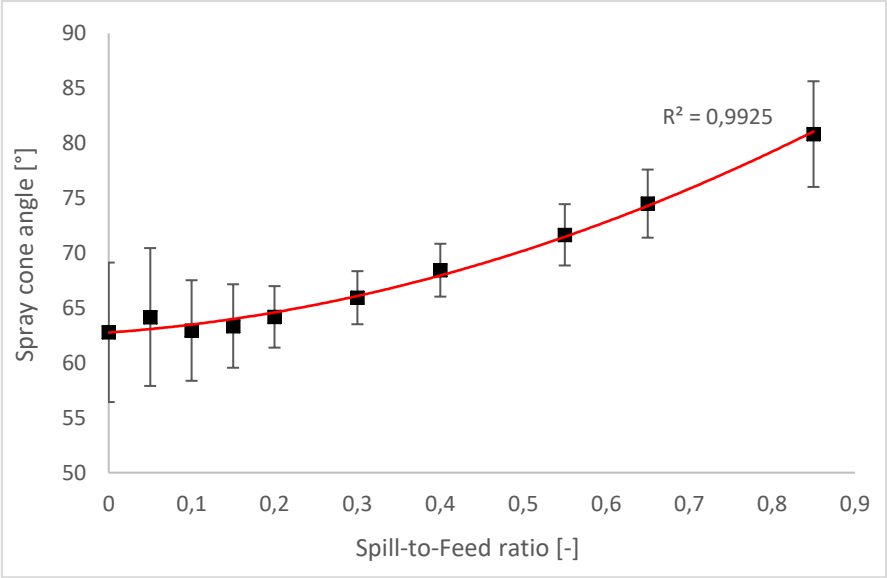

Figure 6-33 The SCA in dependence on SFR, SR atomizer, kerosene

The original and scaled type of SR atomizer were compared in Figure 6-34 A comparison of the original and scaled atomizer, 1 MPa, keroseneFigure 6-34 at 1 MPa of inlet pressure, and three SFR values. The curves for the original and scaled atomizer almost overlap, so the SCA's are practically the same for each regime. Tab. 6-3 shows that each time the SFR increases, the SCA rapidly widens. However, in both cases, the deviation does not exceed 5%.

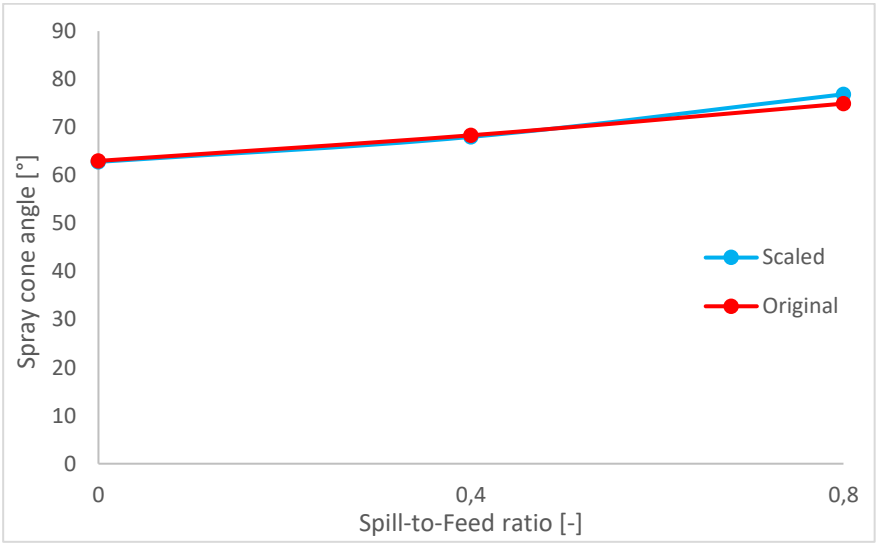

Figure 6-34 A comparison of the original and scaled atomizer, 1 MPa, kerosene

Tab. 6-3 Opening the spill-line of SR atomizer, 1 MPa, kerosene

	Original atomizer	***Scaled atomizer***
SFR [-]	**SCA [°]**	**SCA [°]**
0	63.00	62.80
0.4	68.33	68.00
0.8	74.92	76.86

7 Conclusion

The internal and external flow of both Simplex and SR atomizer was examined theoretically and experimentally. The measurements were performed using LDA and high-speed camera.

The velocity profiles of the Simplex atomizer were found to be almost independent of axial distance and had a sharp maximum near the air core boundary. The air core was stable, fully developed, and cylindrically shaped with little enlargement inside the exit orifice. Its diameter was found independent of operating conditions. The air core fluctuations were observed at the top of the swirl chamber. On the contrary, the SR atomizer produced the internal flow without the air core, so the velocity maximum was lower with a flatter peak at similar *Re* values.

A simple numerical model was developed to estimate the flow field inside the atomizer by particle tracking. It was performed on the basis of high-speed images of the scaled Simplex atomizer with using p-Cymene as a working liquid. The results indicate that the particles move along spiralling-helical trajectories from the top of the swirl chamber to the exit orifice. The number of the particle turns is not governed by any rules; it is not dependent on either the rotation radius or the inlet pressure. It could be probably caused due to a different initial velocity of each particle and a different angle and direction at which the particle enters the swirl chamber. The calculated velocity profiles of single particles were in accordance with the measurement. However, some particles moving in the opposite direction (from the bottom to the top) were also noticed from the high-speed images. This can be atributed to the rotation of the air core around its axis at high speed which creates a flow similar to the tornado phenomenon with a strong central updraft.

The increasing inlet pressure led to a slow widening of the spray cone angle. It was no more than 2° in the case of Simplex atomizer, and 5° for SR atomizer respectively. These different values are caused by fluctuations of the spray, which are strongly affected by the air core stability. The scaled atomizer does not affected the SCA; the deviation did not exceed 1% relative to the original atomizer.

The breakup length of the liquid sheet was found to rapidly decrease with increasing pressure for the Simplex original atomizer. The breakup began much earlier in the case of SR atomizer, and the differences across the pressure range were very small. The standard deviation significantly varied at low pressures, where low aerodynamic forces dominate, so every little difference in sheet thickness strongly affects the change in the breakup length.

Bibliography

[1] Janáčková, L., 2016, "Visualization of liquid breakup from atomization nozzles", Bachelor's thesis, Brno University of Technology, Brno.

[2] Crowe, C., 2006, "Multiphase Flow Handbook", Taylor & Francis, Boca Raton. ISBN 10: 0-8493-1280-9.

[3] Byvel, L., and Orzechowski, Z., 1993, "Liquid Atomization", USA, ISBN 0-89116-959-8.

[4] Lefebvre, A. H., 1989, "Atomization and sprays", Hemisphere Pub. Corp., New York. ISBN 0-89116- 603-3.

[5] Malý, M., 2016, "Experimental study of spray characteristics and functionality of small pressure-swirl atomizers", Master's thesis, Brno University of Technology, Brno.

[6] Rizk, N. K., and Lefebvre, A. H., 1985, "Spray Characteristics of Spill-Return Atomizers", Journal of Propulsion and Power 1 (3).

[7] Biswas, G., and Som, S. K., 1986, "Coefficient of discharge and spray cone angle of a pressure nozzle with combined axial and tangential entry of power-law fluids", Applied scientific research, 43.1., 3-22.

[8] Taylor, G. I., 1948, "The Mechanics of Swirl Atomizers", International Congress of Applied Mechanics 2, pt. 1, London, pp. 429-432.

[9] De Corso, S. M., Kemeny, G. A., and Pittsburgh, E., 1957, "Effect of Ambient and Fuel Pressure on Nozzle Spray Angle", Transf. of ASME 79.3, 607-615.

[10] Rizk, N. K. and Lefebvre, A. H., 1985, "Prediction of Velocity Coefficient and Spray Cone Angle for Simplex Swirl Atomizers", International Journal of Turbo and Jet Engines, 4 (1-2), pp. 65-74.

[11] Chinn, J. J., 1996, "The Internal Flow Physics of Swirl Atomizer Nozzles", Doctoral dissertation, University of Manchester: UMIST.

[12] Chinn, J., and Yule, A., 1996, "Computational Analysis of Swirl Atomizer Internal Flow", University of Manchester, England.

[13] Som, S. K., and Mukherjee, S. G., 1980, "Theoretical and experimental investigations on the formation of air core in a swirl spray atomizing nozzle", India.

[14] Datta, A., and Som, S. K., 2000, "Numerical prediction of air core diameter, coeficient of discharge and spray cone angle of a swirl spray pressure nozzle", International Journal of Heat and Fluid Flow 21, 412-419.

[15] Khavkin, Y. I., 2003, "Theory and practice of swirl atomizers", CRC Press, University of Minnesota, USA.

[16] Halder, M. R., Dash, S. K., and Som, S. K., 2002, “Initiation of air core in a simpley nozzle and the effects of operating and geometrical parameters on its shape and size”, Experimental and Fluid Science 26, 871-878. India.

[17] Lee, S., Kim, W., and Yoon, W., 2010, “Spray formation by a swirl spray jet in low speed cross-flow”, Journal of Mechanical Science and Technology 24 (2), 559-568.

[18] Löffler-Mang, M., and Leuckel, W., 1991, “Atomization with spill-controlled swirl pressure-jet nozzles”, ICLASS, USA.

[19] Altieri, A., Acharya, L., and Cryer, S. A., 2014, “Mechanisms, experiment, and theory of liquid sheet breakup and drop size from agricultural nozzles”. New York, Atomization and Sprays 24.

[20] Som, S. K., 1983, “Theoretical and Experimental Studies on the Formation of an Air Core in a Swirl Spray Pressure Nozzle Using a Power Law Non-Newtonian Liquid”, Applied Scientific Research 40, 71-91.

[21] Ashgriz, N., and SpringerLink (Online service), 2011, “Handbook of atomization and sprays: Theory and applications”, Springer, New York, pp. xvi, 935 p.

[22] Horvay, M., and Leuckel, W., 1984, “LDA-Measurements of Liquid Swirl Flow in Converging Swirl Chambers with Tangential Inlets”.

[23] Horvay, M., and Leuckel, W., 1986, “Experimental and Theoretical Investigation of Swirl Nozzles for Pressure-Jet Atomization”, Ger. Chem. Eng. 9, 276-283.

[24] Cooper, D., Yule, A., and Chinn, J., 1999, “Experimental Measurements and Computational Predictions od the Internal Flow Field in a Pressure Swirl Atomizer”, ILASS-Europe, Toulouse.

[25] Krämer, M., Horvay, M., Löffler-Mang, M., and Leuckel, W., 1987, “Velocity profile measurements within swirl pressure-jet nozzles using L.D.A.”. Laser anemometry – advances and applications, UK.

[26] Hansen, K. G., and Madsen, J., 2001, “A Computational and Experimental Study of the Internal Flow in a Scaled Pressure-Swirl Atomizer”, M.Sc. Thesis, Aalborg Universitet Esbjerg, Aalborg.

[27] Rayleigh, L., and Strutt, J., 1878, “On the instability of jets”, Proc. London Math. Soc. 10, pp. 4-13.

[28] Weber, C., 1931, “On the disruption of liquid jets”. Math. Mech. 2.

[29] Lin, S. P., 2003, “Breakup of liquid sheets and jets”, Cambridge University Press.

[30] Jeng, S. M., Jog, M. A., and Benjamin, M. A., 1998, “Computational and Experimental Study of Liquid Sheet Emanating from Simpley Fuel Nozzle”, AIAA Journal 36 (2).

[31] Cooper, D., and Yule, A. J., 2001, “Waves on the Air Core Liquid Interface of a Pressure Swirl Atomizer”, ILLASS-Europe, Zurich.

[32] Donjat, D., Estivalezes, J. L., and Michau, M., 2002, “A Description of the Pressure Swirl Atomizer Internal Flow”, Proceedings of ASME, Canada.

[33] Kenny, R. J., Hulka, J. R., Moser, M. D., and Rhys, N. O., 2009, “Effect of Chamber Backpressure on Swirl Injector Fluid Mechanics”, Journal of Propulsion and Power 25 (4).

[34] “Laser Doppler Anemometry”, Massachusetts Institute of Technology, [Online], http://web.mit.edu/

[35] Frohn, A., and Roth, N., 2000, “Dynamics of Droplets”, Springer, Germany. ISBN 3-540-65887-4.

[36] Russo, F., and Basse, N. T., 2016 “Scaling of turbulence intensity for low-speed flow in smooth pipes”, Flow Measurement and Instrumentation 52.

[37] “TSI – Precision Measurement Instruments”, [Online], http://www.tsi.com/.

[38] Dantec Dynamics, 2011, “LDA and PDA Reference Manual”, Denmark, Publication no.: 9040U1312.

[39] Jedelsky, J., Maly, M., Pinto del Corral, N., Wigley, Janackova, L., G., and Jicha, M., 2018, “Air-liquids interactions in a pressure-swirl spray”, International Journal of Heat and Mass Transfer

[40] Guy, S. R. D., 2008, “Optical patternation of fuel sprays in a gas turbine combustion chamber under operationally representative flow conditions”, Canada, ISBN: 978-0-494-42122-2.

[41] Novotny, J., and Manoch, L., 2012, “The criterion of choosing the proper seeding particles”, Engineering Mechanics 18.

[42] Rafal, J. S., Ritsu, D., and Toshisuke, H., 2000, “Effect of Turbulence on Vaporization, Mixing, and Combustion of Liquid-Fuel Sprays”, Combustion and Flame 120:479-491, Elsevier Science Inc.

[43] Corcoran, T. E., and Chigier, N., 2002, “Inertial Deposition Effects: A Study of Aerosol Mechanics in the Trachea Using Laser Doppler Velocimetry and Fluorescent Dye”, Journal of Biomechanical Engineering 124

[44] Brennen, Ch. E., 2005, “Fundamentals of multiphase flow”, Cambridge Univ. Press.

[45] Yule, A. and Chinn, J. J., 1997, “Pressure Swirl Atomizer Internal Flow and Performance”, UMIST, England.

[46] Maly, M., Jedelsky, J., Slama, J., Janackova, L, Sapik, M, Wigley, G, and Jicha, M., 2018, “Internal flow and air core dynamics in Simplex and Spill-return”, International Journal of Heat and Mass Transfer

[47] Zhang, Z., 2010, “LDA Application Methods: Laser Doppler Anemometry for Fluid Dynamics”, Springer.

[48] Nieuwkamp, W. C., 1985, “Flow Analysis of a Hollow Cone Nozzle with Potential Flow Theory”, International Conference on Liquid Atomization and Spray Systems, Chicago, USA.

[49] Moon, S., Abos-Serie, E., and Bae, C., 2009, “Air flow and pressure inside a pressure-swirl spray and their effects on spray development”, Experimental Thermal and Fluid Science 33, 222-231.

[50] Sumer, B., Erkan, N., Uzol, O., and Tuncer, I. H., 2012, “Experimental and Numerical Investigation of a Pressure Swirl Atomizer”, ICLASS, Germany.

[51] Maly, M., and Janackova, L., 2018, “Numerical simulation of internal flow field of the pressure-swirl atomizer”, Brno University of Technology

[52] “Realisticky.cz”, [Online], http://www.realisticky.cz/

[53] Yule, A. J., Sharief, R. A., Jeong, J. R., Nasr, G. G., and James, D. D., 2000, “The Performance Characteristics of Solid-Cone-Spray Pressure-Swirl Atomizers”, Atomization and Sprays 10, pp. 627-646.

[54] Senecal, P. K., Schmidt, D. P., Nouar, Rutland, C. J., Reitz, R. D., and Corradini, M. L., 1999, “Modeling high-speed viscous liquid sheet atomization”, International Journal of Multiphase Flow 25, 1073-1097, Madison, USA.

[55] Goodwin, M., 2004, “Transient liquid sheets and their relationship to GDI sprays”, Loughborough University

[56] Kutty, P. S., Narasimhan, M. V., and Narayanaswamy, K., 1978, “Design and Predistion of Discharge Rate, Cone Angle and Aircore Diameter of Swirl Chamber Atomisers”, International Conference on Liquid Atomization and Spray Systems, Tokyo, Japan.

List of symbols

Roman symbols

A_o	Cross-section of the discharge orifice	[m^2]
A_p	Cross-section of the inlet ports	[m^2]
b_p	Width of the inlet tangential port	[m]
C_C	Cunningham slip correction factor	[-]
C_D	Discharge coefficient	[-]
D	Characteristic geometric dimension	[m]
d_a	Diameter of the air core	[m]
d_o	Diameter of the exit orifice	[m]
d_p	Particle diameter	[m]
d_s	Width/diameter of the swirl chamber	[m]
d_{so}	Siameter of the spill-line orifice	[m]
f	Frequency	[Hz]
f_D	Frequency of the Doppler signal	[Hz]
F_r	Froude number	[-]
g	Gravitational acceleration	[m/s^2]
h_p	Height of the inlet tangential port	[m]
h_s	Height of the swirl chamber	[m]
K	Atomizer constant	[-]
k_{vel}	Correction coefficient of measured velocity	[-]
m_l	Liquid mass flow rate	[kg/s]
L_b	Breakup length	[m]
l_o	Length of the exit orifice	[m]
l_p	Length of the tangential inlet port	[m]
l_{so}	Length of the spill-line orifice	[m]
n_1	Refractive index of Plexiglass	[-]
n_2	Refractive index of kerosene	[-]
Oh	Ohnesorge number	[-]
Q	Volume flow rate	[m^3/s]
R	Radius of the atomizer at the plane where the particle is located at the time t	[m]
R_s	Radius of the swirl chamber at the measurement plane	[m]

R_{ac}	Radius of the air core	[m]
r_o	Radius of the exit orifice	[m]
r_{oac}	Radius of the air core in the exit orifice	[m]
r_s	Radius of the swirl chamber	[m]
r(t)	Local radius of the particle	[m]
$r_{(t0)}$	Initial radius of the particle	[m]
Re	Reynolds number	[-]
Re_{crit}	Critical Reynolds number	[-]
Re_o	Reynolds number of the exit orifice	[-]
s_1	Virtual distance of the measurement volume from the atomizer wall	[m]
s_2	Real distance of measurement volume	[m]
S	Dimensionless air core radius in the exit orifice	[-]
S_N	Swirl number	[-]
$S_{(t)}$	Cross-section area of the atomizer at the plane where the particle is located at the time t	[m^2]
Stk	Stokes number	[-]
t	Time	[s]
Δt	Time differential	[s]
t_o	Liquid sheet thickness in the exit orifice	[m]
v_x	Velocity of particle on the x-axis (LDA)	[m/s]
v_{x_Mean}	Mean value of velocity	[m/s]
v_{x_RMS}	Root mean square velocity	[m/s]
v	Characteristic velocity	[m/s]
v_a	Axial velocity component	[m/s]
$\overline{v_i}$	Mean velocity in the inlet ports	[m/s]
v_r	Radial velocity component	[m/s]
v_t	Tangential velocity component	[m/s]
$\overline{v_{tp}}$	Mean tangential velocity of particle or droplet	[m/s]
v_0	Initial velocity of particle	[m/s]
We	Weber number	[-]
We_g	Gas Weber number	[-]
We_{gc}	Critical gas Weber number	[-]
X	Coordinate in X direction	[m]

Y	Coordinate in Y direction	[m]
Z_i	Coordinate in Z direction	[m]

Greek symbols

Δp	Pressure differential	[Pa]
δ_f	Fringe distance	[m]
ε	Angular acceleration	[rad/s^2]
η	Atomizer efficiency	[-]
θ_b	Angle between the incident laser beams	[°]
θ	Half of the spray cone angle	[°]
λ	Wavelength of the laser light	[m]
μ_l	Dynamic viscosity	[Pa·s]
π	Ludolph's number	[rad]
ρ_l	Liquid density	[kg/m^3]
ρ_g	Gas (air) density	[kg/m^3]
ρ_p	Particle/droplet density	[kg/m^3]
σ_l	Surface tension	[kg/s^2]
φ	Angle of rotation	[rad]
φ_0	Initial angle of rotation	[rad]
ω	Angular velocity	[rad/s]
ω_0	Initial angular velocity	[rad/s]

Abbreviations

CCD	Charge Coupled Device
FFT	Fast Fourier transformation
LDA	Laser Doppler anemometry
LDV	Laser Doppler velocimetry
LED	Light Emiting Diode
LIF	Laser induced fluorescence
PDA	Phase Doppler anemometry
PIV	Particle Image Velocimetry
PS	Pressure-swirl
RMS	Root-mean-square

SCA	Spray cone angle
SFR	Spil-to-feed ratio
SR	Spill-return
Std	Standard deviation
TI	Turbulence intensity